3-30-2022 1:30 PM

The electrical, thermal, and morphological properties of microinjection-molded polypropylene nanocomposites

Renze Jiang, *The University of Western Ontario*

Supervisor: Hrymak, Andrew N., *The University of Western Ontario*

A thesis submitted in partial fulfillment of the requirements for the Master of Engineering Science degree in Chemical and Biochemical Engineering

Abstract

Microinjection molding (μIM) exhibits significantly higher shear rates and faster cooling rates, as compared to conventional injection molding, which affect the characteristics of its final products. The effect of carbon black (CB), carbon nanotubes (CNT), and graphene nanoplatelet (GNP) fillers on the electrical conductivity properties of microinjection-molded polypropylene (PP) nanocomposites was systematically studied. Results showed the electrical conductivity properties of PP/CNT and PP/CB microparts were significantly influenced by mold geometry. PP/CNT/CB hybrid filler microparts demonstrated synergistic increases in electrical conductivity and crystallization temperature with higher CNT loading. Morphological observations indicated significant CB and CNT phase separation. Powder-PP/GNP composites exhibited higher electrical conductivity compared to pellet-PP/GNP due to the similar particle size between PP powder and GNP flakes promoting more uniform microscopic dispersion. Moreover, 'precoated' samples exhibited smaller GNP flake size, better microscopic dispersion and exfoliation of GNP fillers.

Keywords

Microinjection molding; Polymer composites; Carbon fillers; Hybrid fillers; Electrical conductivity; Microstructure

Summary for Lay Audience

There is a significant demand for small scale microinjection molded parts in the fields of electronics, automotive, and medical industries, with a special focus on microelectromechanical systems (MEMS). Microinjection molding (μIM) is a promising technology with many advantages such as high efficiency for mass production, low cost, excellent process control, and a wide selection of thermoplastics that can be used to manufacture micro-components. Since microinjection molding is significantly different than many existing processes, there is a need to study how the process affects the material properties of the finished microparts produced through this method. Recent studies have characterized the properties of carbon-filled polymer composite microparts. However, further studies are required to understand more complex systems. The following results were obtained in the present study:

First, it was found that the mold geometry can significantly affect the distribution of carbon fillers within the microparts, and consequently, the electrical and thermal properties of the entire microparts.

Second, adding two types of carbon fillers concurrently (e.g., carbon black and carbon nanotubes) to polypropylene plastic can result in synergistic improvements to electrical conductivity and thermal properties of the microparts under certain conditions.

Third, using various pretreatment methods to prepare the composite materials before microinjection molding can significantly improve the properties of produced microparts. For example, ‘precoating’ the fillers on the surface of polypropylene powder through solvent blending and ultrasonication resulted in better filler distribution, smaller particle size and more numerous filler particles.

As a result of findings from this research, future commercially produced microparts can incorporate some of the aforementioned strategies to improve the electrical, thermal, and morphological properties of microinjection molded polymer composites.

Acknowledgments

I would like to express my most sincere gratitude and thanks to my supervisor, Prof. Andrew Hrymak, for his wisdom and continuous support throughout the completion of my project. I am amazed by his attitude and insight into both academic research and everyday life. I would like to thank my new group member, Piyush Lashkari, for his support throughout the second half of my studies, and for his help with the GNP molding experiments under my training and guidance.

The thesis would be impossible without the generous help and support from my colleagues and friends, especially in light of lab and equipment access challenges due to COVID-19. In particular, I would like to thank Shengtai Zhou (Sichuan University) for his training to operate the Battenfeld Microsystem 50 machine and for providing many DSC (sections 3.1 and 3.2), TGA (sections 3.1 and 3.2), melt rheology (section 3.2), and SEM (sections 3.2 and 3.3) raw data used in this thesis. I also want to acknowledge Mr. Ian Vinkenvleugel (University Machine Services, the University of Western Ontario) for his assistance in repairing the Battenfeld machine and for swapping mold inserts, Mr. Dicho Zomaya (Department of Chemical and Biochemical Engineering) for assisting in running the DSC tests for section 3.3 of this thesis, and Mr. Brad Kobe (Surface Science Western) for providing SEM images for section 3.1 of this thesis. I would like to thank Denys Vidish and Prof. Giovanni Fanchini for helping me to explore and understand the different ways to carry out my graphene experiments.

Due to the unprecedented disruption and challenges caused by COVID-19, I would also like to acknowledge external, non-academic support that I received during this difficult time. I would like to thank Nicholas Everdell, Prof. Jose Herrera, Beth Prysnuk, Whitney Barrett, and members of the Society of Graduate Students for their advice, support, and counselling.

Lastly, I would like to thank my friends and family for their love, support, and encouragement throughout my studies.

Table of Contents

List of Tables

List of Figures

List of Symbols

T_d	The initial decomposition temperature
T_5	The 5wt% decomposition temperature
T_{30}	The 30wt% decomposition temperature
T_{max}	The maximum decomposition temperature
R_{560}	Char residue at 560°C
wt%	Weight percent
χ_c	percent crystallinity
T_m	melting temperature
T_c	crystallization temperature
Ω	Ohm
σ	Volumetric clectrical conductivity
p_c	Percolation threshold
G'	Storage modulus
G''	Loss modulus
η *	Complex viscosity
S	Siemens

List of Abbreviations

μIM	Microinjection molding
MEMS	Microelectromechanical systems
CIM	Conventional injection molding
CM	Compression molding
CB	Carbon black
CNT	Carbon nanotubes
SWCNT	Single-walled nanotubes
MWCNT	Multiwalled nanotubes
0D	Zero-dimensional
1D	One-dimensional
2D	Two-dimensional
3D	Three-dimensional
CVD	Chemical vapor deposition
GIC	Graphene-intercalated compounds
GNP	Graphene nanoplatelets
GO	Graphene oxide
PLA	Polylactic acid
PMMA	Poly(methyl methacrylate)

PP	Polypropylene
PET	Polyethylene terephthalate
rGO	Reduced graphene oxide
g-MA-PP	Maleic anhydride-grafted polypropylene
CNC	Computerized Numerical Control
TGA	Thermogravimetric analysis
DC	Direct current
FD	Flow direction
TD	Transverse direction
DSC	Differential scanning calorimeter
SEM	Scanning electron microscopy
TGA	Thermogravimetric analysis
CT	Computed tomography

Chapter 1

1 Introduction

1.1 Motivation

There has been an increasing demand for injection molded parts, mostly in the electronics, automotive, and medical industries. More recently, micro-injection systems (μIM) are becoming more prevalent, with a renewed focus on microelectromechanical systems (MEMS) [1]. Micro-injection molding is becoming an important technology to fabricate miniature products and components, which possess many advantages such as high efficiency for mass production, low cost, and excellent process control [2]. Because of these factors, the adaptation of μIM process to microfabrication will lead to a promising technology for MEMS applications [3], [4]. Polymer composites are often used as molding materials due to their weight advantage, processability, and resistance to wear and corrosion [4], but other materials such as metal, glass, quartz, and silicon can also be used for the manufacturing micro-components [5].

As a miniaturized version of conventional injection molding (CIM), μIM shares similar procedures with CIM, including plasticization, metering, injection, cooling, and ejection. However, μIM is not merely a scaled downed version of CIM, with several notable differences, all of which might significantly affect the characteristics of micromolded products:

1. Extremely high shearing effects in μIM might cause different filler distribution in composite materials when compared to CIM [6]
2. Microscale rheological behavior might significantly influence the material properties of microparts in μIM, whereas it is a negligible factor in CIM [7]
3. Extremely high pressure can result in non-negligible melt compressibility [8]
4. Reduced thickness and higher aspect ratio of μIM microparts results in much higher shear deformation and cooling rates when compared to CIM [9]

There is a large body of research aimed at incorporating carbonaceous fillers into various polymer matrices [10]–[15]. However, much of existing studies on polymers composites and processing were carried out using hot press and CIM, which are different than μIM filled polymer flows. For example, Jiang et al. [16] reported there is no obvious flow-direction orientation of CNT fillers in samples produced through conventional injection molding, but very prominent FD-orientation of fillers in μIM microparts. This can be attributable to the extremely high shearing rate of up to 10^6 in μIM, which would preferentially align fillers along the flow direction [8]

Moreover, previous studies showed that polymer composites produced through compression molding (CM) exhibit far superior electrical conductivity compared to parts produced through CIM [17] and μIM [18], [19]. There is a need to examine methods to further study and improve the properties of micromolded composite materials.

1.2 Carbon Fillers

1.2.1 Carbon Black

Among all the conductive fillers, carbon black is widely used due to its abundance in nature and low price, with many potential applications including but limited to conductive ink, coating, fuel cells, electromagnetic shielding, and sensors [15], [20], [21]. There are many factors that affect the conductivity of CB-filled polymer composites. For example, Balberg [22] argued that the electrical percolation threshold of CB-based polymer composites (defined as the critical concentration of filler where the composite material quickly turns from an insulator into a conductor) is strongly related to the structure of CB fillers used and the molding conditions. Huang [23] reported that CB with smaller diameter and higher surface area, as well as greater porosity, are more electrically conducive in CB-filled polymer composites. Additionally, crystallization can also affect the formation of conductive pathways. Yu et al. found that slower crystal growth could help to form CB aggregates in amorphous regions of a PP matrix, and thus be less likely to be trapped in crystalline regions where they could not participate in the formation of conductive pathways [24].

1.2.2 Carbon Nanotubes

Carbon nanotubes can be viewed as graphene nanosheets rolled up into a cylindrical shape of about 10 nm in diameter, capped by half of a fullerene-like shape at each end [25]. The remarkable properties of carbon nanotubes (CNT) attracted intense interest from the scientific community since the pioneering work by Sumio Iijima in 1991 [26], with a plethora of journal articles and patents covering various topics of CNT production, functionalization, applications, fabrication and characterization of CNT-filled polymer nanocomposites [13].

There are two main types of carbon nanotubes. Single-walled nanotubes (SWCNT) consist of a single graphene sheet seamlessly wrapped into a cylindrical tube. Multiwalled nanotubes (MWCNT) are comprised of multiple concentrically nested nanotubes [27]. The terms ‘zigzag’ and ‘armchair’ refer to the arrangement of hexagons around the circumference of the circumference of the CNT, while ‘chiral’ denote hexagons that are arranged helically around the axis of CNTs, as shown in Figure 1 below [25].

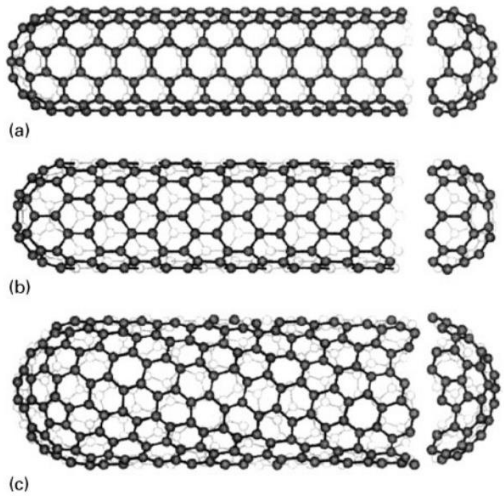

Figure 1: Three configurations of carbon nanotube structures: (a) armchair (b) zigzag (c) chiral [25].

Thanks to its exceptional electrical and thermal conductivities, mechanical properties, and high aspect ratio, CNT is frequently utilized as carbon filler to enhance to

properties of polymers [10], [13]–[15]. For example, CNTs have demonstrated the potential for being used as electrical conductors [28] and reinforcements in high strength, light weight, high-performance composites [29]. However, poor interfacial interaction between CNT and host polymers, the state of CNT dispersion in the polymer matrices, and the processing techniques all significantly affect the expected benefit of adding CNT fillers [10]. Additionally, due to the poor yield and costly fabrication and purification process, the price of CNT is still quite high, which limits its commercial applications [30], [31].

Dispersion:

There are three main factors to the dispersion CNT-based nanocomposites. The first factor is the disentanglement of CNT agglomerates at the nano-level, the second factor is on the microscopic dispersion, and the third is the aspect ratio of CNTs. One study suggested that the initial breakup of large CNT agglomerates is dependent on the ultrasonication power, while the overall quality of the microscopic dispersion is more dependent on the cumulative energy input [32]. Skipa and coworkers argued that the reason for low electrical conductivity of many CNT-composites is due to insulating polymers wrapped around CNT rods, thus preventing the fillers from forming a conductive network. Therefore, instead of a uniform microscopic dispersion, selective agglomeration might be desirable [33].

Role of Aspect Ratio:

Despite having very high theoretical aspect ratios, in reality, CNTs tend to form agglomerates and entangled tube bundles. This lowers the effective aspect ratio of CNTs, which results in a higher experimental electrical percolation threshold than the theoretically expected values for fully elongated CNTs [33]. Moreover, this is compounded by the problem that dispersed CNTs, without sufficient surface functional groups, tend to agglomerate because of van der Waals and Coulomb attractions [34] in subsequent processing such as injection molding. Consequently, many researchers have attempted to disentangle CNT in polymer matrices, which in turn results in more even distribution of CNT fillers.

However, excessive processing can negatively affect the properties of CNT-based composites. Ultrasonication and ball-milling techniques were found to reduce the length of CNTs, while magnetic agitation, shear mixing, and chemical modification did not [35]. Thus, a good balance of loosely entangled on the nanoscopic level but uniformly distributed CNT secondary agglomerates on a microscopic level is most desirable for enhancing electrical conductivity. It's a delicate balancing act of achieving better dispersion versus maintaining a high aspect ratio. For example, one study suggested that CNTs with very low aspect ratios are less effective in forming conducting networks despite good dispersions; with high CNT aspect ratio, better CNT dispersion is the dominant factor [36].

There are also similarities between the effect of CNT and GNP processing on filler aspect ratios. For example, CNT could be damaged and broken into smaller pieces during ball-milling [37] and ultrasonication [38], [39]; similar results were also reported for GNP [40]. This is further supported by one study that adapted the interparticle distance (IPD) theory used in CNT towards GNP particles with good predictability; aspect ratio was found to be a predominant factor of the nanocomposite percolation threshold [41].

1.2.3 Graphene

Graphene is a flat monolayer of carbon atoms tightly packed into a two-dimensional (2D) honeycomb lattice, completely conjugated sp2 hybridized planar structure. It is the basic building block for carbon allotropes of other dimensions. For example, graphene can be wrapped up into 0D fullerenes, rolled into 1D nanotube or stacked into 3D graphite, as illustrated in the figure below [42].

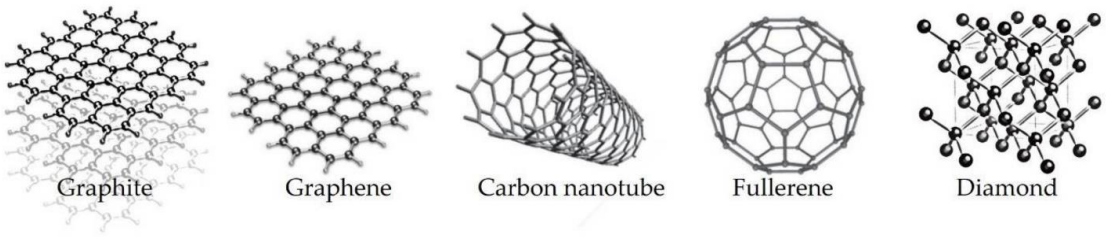

Figure 2: Different Allotropes of Carbon. From Left to Right: Graphite (3D), Graphene (2D), CNT (1D), Fullerene (0D), and Diamond (3D) [42].

Over the last decade, graphene has been extensively investigated as an alternative carbon-based nanofiller in the preparation of polymer nanocomposites, with the potential of exhibiting great mechanical and electrical properties [43]. There are many studies exploring the use of graphene and graphene derivatives in biomedical applications such as cellular and tissue engineering [44]. Graphene-based nanocomposites are suitable for wearable health monitoring sensors due to their thin, flexible, and sensitive nature [45], but also mechanically robust enough to be used to fabricate lightweight, thin, and low-cost flexible electronics [46] and light-weight components for aerospace applications [47].

Synthesis and Exfoliation:

The original technique used to discover and discover single-layer graphene in 2005 was the micromechanical cleavage of bulk graphite, which is also known as the 'Scotch tape' method [48]. This method can provide high-quality graphene crystallites for most research purposes [49]. The chemical vapor deposition (CVD) process has been extensively studied as a method to synthesize uniform films of monolayer and few layers graphene [50], [51]. Chemical methods for the synthesis of graphene involve two steps. The first step is to use graphene-intercalated compounds (GIC) to increase interlayer spacing, and then the expanded graphite is exfoliated to produce few layers graphene with high temperature or ultrasonication [52]. Some additional methods include epitaxial growth of graphene on electrically insulating surfaces [53] and using colloidal suspension to produce chemically modified graphene [54].

The importance of graphene exfoliation cannot be overstated. For instance, the thermal conductivity of single-layer graphene can reach about 5000 $W \cdot m^{-1} \cdot K^{-1}$ [55] for single layer, and drops to 2800 $W \cdot m^{-1} \cdot K^{-1}$ for 2 layers and 1300 $W \cdot m^{-1} \cdot K^{-1}$ for 4 layers [56]. This shows the significant impact of graphene exfoliation on the thermal conductivity. Additionally, a high degree of exfoliation usually leads to a greater number

of GNPs in a polymer melt, both of which could accelerate the formation of GNP conductive networks. Graphene flake size can also significantly influence various thermal and mechanical properties [57]. Many commercially available GNP flakes, such as Grade M produced by XG Science, can be produced through chemical intercalation of natural graphite followed by thermal exfoliation. Given a monolayer thickness of 0.335 nm and interlayer distance of 0.14 nm [58], this roughly translates to few layers to few dozen layers thick graphene flakes, depending on the product grade.

Moreover, if the graphene sheets are not well separated from each other, graphene sheets will tend to agglomerate after exfoliation, and sometimes even undergo restacking back into small graphite particles due to Van der Waals interactions [59]. One method to prevent agglomeration is by attaching other small molecules or polymers to the graphene sheets. For example, hydrophilic or hydrophobic groups prevents aggregation of graphene sheets because of either polar-polar interactions or bulky size [60]. Similarly, functionalizing the graphene can also aid the dispersion in a hydrophilic or hydrophobic media, as well as in the organic polymer [61]. Controlling the crystallization process of polyolefins can also be beneficial towards controlling the dispersion state [62], which in turn affects dispersion state and agglomeration.

1.2.4 Hybrid Fillers System

Graphene/Carbon Nanotubes:

Theoretically, perfectly dispersed graphene should have a lower percolation threshold and a higher electrical conductivity than CNT [63]. In reality, graphene-based composites often have a higher percolation threshold and a lower electrical conductivity compared to CNT, which can be partially attributed to significant, large size GNP agglomeration and stacking in GNP-filled polymer nanocomposites due to van der Waals forces and strong π–π interactions between the GNP sheets [64]; GNP flakes are more likely to aggregate than CNT due to large plane-to-plane surface area. Additionally, as a two-dimensional material, GNP is more difficult to interlock with each other into a 3D conductive network structure than is CNT [65].

Thus, using a hybrid fillers system comprised of GNP and CNT might provide superior conductivity over a GNP single filler system because graphene nanoplatelets could improve CNT dispersion and suppress aggregation due to their large surface area and space hindrance effects [66]. At the same time, CNT rods could also reduce the formation of large size stacking of GNP sheets [67]. Additionally, synergetic effects in electrical conductivity may arise from the presence of the flexible MWCNT rods, which favor the bridging of planar GNP nanoplatelets and thus facilitating the formation of a 3D network [68]. CNT rods can act as 'bridges' to enhance electron transport across GNP sheets and nanotubes, and thus significantly increase the electrical conductivity of the composites. For example, Fan et al. [69] reported that a hybrid filler system comprised of MWCNT and graphene oxide (GO) resulted in better dispersion than either a GO or MWCNT single filler system due to the introduction of 1D MWCNT between the 2D graphene sheets, with a resulting 3D network structure that helps to inhibit the aggregation of graphene sheets. Moreover, it has been well-documented that subjecting CNT to ultrasonication will reduce its aspect ratio [38], [39], and the large flat surface of GNP can also provide a shielding mechanism to protect MWCNT from damage and fragmentation caused by high-power ultrasonic vibration, which helps to preserve the excellent aspect ratio of CNT and enhance electrical conductivity [70].

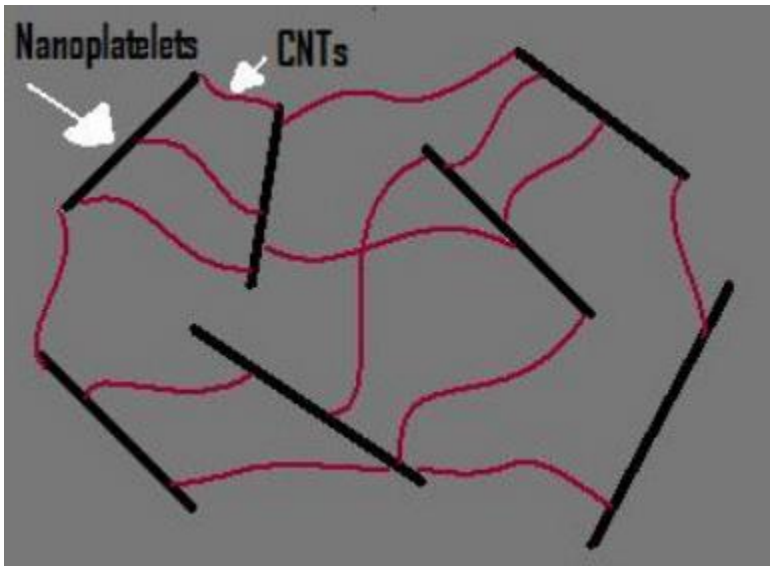

Figure 3: CNT branching out acting as conducting channels between graphene nanoplatelets taken from a literature source [70]

There are also many works that examine the effect of the CNT:GNP ratio. Ivanov et al. found that adding CNT/GNP to polylactic acid (PLA) with equal or greater CNT loading than GNP loading resulted in a synergetic effect on the electrical conductivity, with the values higher than those observed of single filler systems [71]. Another study argued that the ideal CNT:GNP ratio is 4:1 in some epoxy-based composite resins [67]. However, adding a small amount of CNT, e.g., a CNT:GNP ratio of 1:10, is sufficient to lead to decrease percolation threshold by 50% and increase electrical conductivity by several orders of magnitude. [68]

Carbon Black/Carbon Nanotube:

It is also possible for CB and CNT fillers to work synergistically to improve the electrical conductivity of polymer composites. Al-Saleh reported a synergistic effect that was greatest at a CNT75:CB25 hybrid filler ratio using a hot press [72]. Sumfleth et al. reported that epoxy/(CNT50:CB50) ternary filler systems exhibited comparable electrical properties to epoxy/CNT binary composites at the same filler loading wt%, but three times lower than the 0.085wt% percolation threshold of the epoxy/CB system [73]. This suggests that CB can be used to replace some CNT while retaining comparable electrical conductivities [74].

One theory is that CNT fillers might help to form conductive networks by creating ‘bridges’ that connect CB agglomerates [75], [76]. At the same time, CB particles can effectively link the gaps present between the unconnected CNTs, resulting in the formation of conducting networks [72], [74]. Another theory is that the distribution and mobility of CNT fillers might be affected by CB particles. This might be favorable for the formation of conductive networks in some composite systems under certain conditions [75]. However, Wu and co-workers argued that in a hybrid system, it is possible to have a segregated CB particle phase and a CNT bridge phase, thus preventing the fillers from effectively constructing synergetic ‘bridging’ effect [75]. Moreover, the electrical conductivity is greater at higher CNT-to-CB ratio because CB aggregates have lower electrical conductivity and aspect ratio than the CNT particles [72].

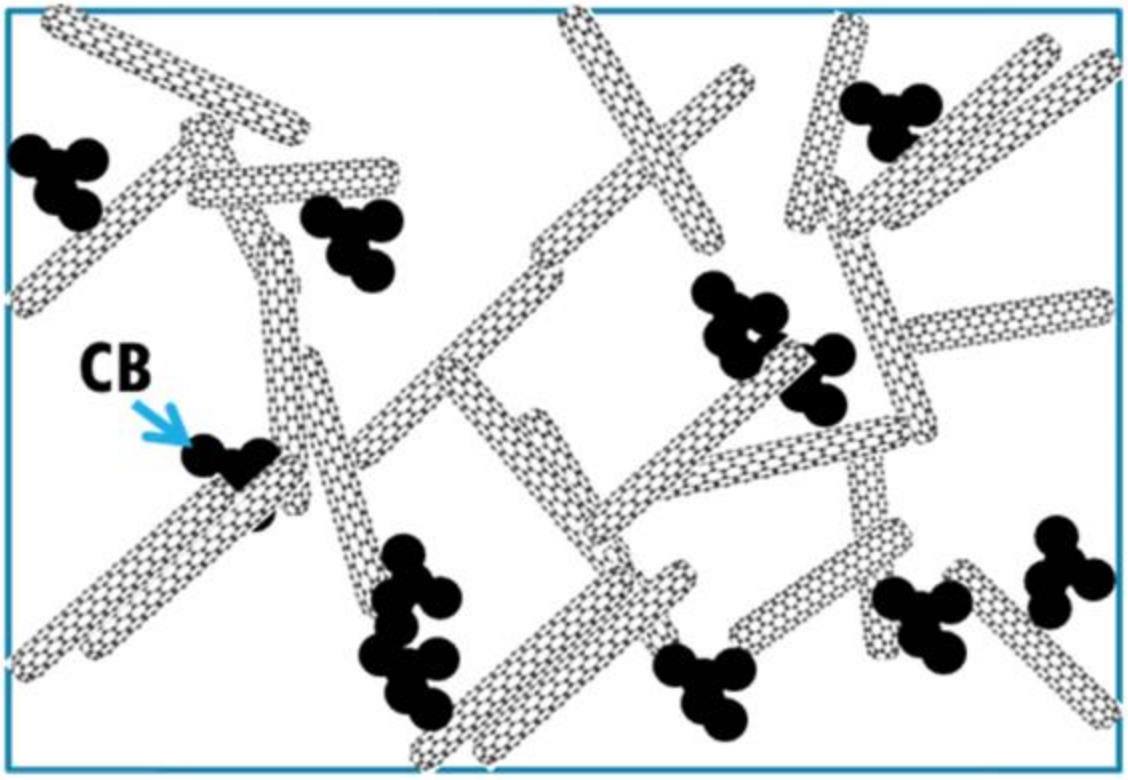

Figure 4: Graphical representation of CNT-CB ‘island-bridging’ in producing synergistic effect to enhance electrical conductivity [72].

1.3 Polymer-Filler Mixing Methods

One of the main challenges in preparing polymer-carbon composites is that many carbon fillers have significant primary agglomeration, which is defined as the natural agglomeration of carbon fillers in their normal storage conditions (not including liquid suspension). Thus, one challenge is to find a way to break up the carbon filler agglomerates before melt compounding to ensure more uniform microscropic and nanoscopic dispersion.

1.3.1 Melt Mixing

Melt processing is the preferred choice for many industrial applications because of its low cost, simplicity, and scalability. The process involves melting solid polymer into viscous liquid form, and then using a high shear force to disperse the nanofillers. Melt blending is popular because it does not require any solvents for the dispersion of

nanofillers, and results obtained from melt blending experiments can be readily transferred to industrial processes such as extrusion and injection molding [77]. Since melt mixing plays a critical role in the practical fabrication of polymer composites, especially in large scale industrial applications, methods to improve the properties of polymer nanocomposites should consider the use of melt [78].

Even though solvent dispersion appears more efficient than melt mixing [79], the latter is much more frequently used at an industrial scale. Huang et al. utilized the traditional melt blending method and reported that an optimal conductivity of 0.36 S/m occurs at 20 wt% loading of graphene nanosheets [80]. Additionally, Beuguel et al. used an internal batch mixer to demonstrate that melt blended, non-exfoliated GNP composites exhibited similar thermal, rheological and mechanical properties compared to nanocomposites based on reduced graphene [81]**.** These studies suggest that melt blending is a viable method for preparing PP/GNP nanocomposites.

However, it has been argued that melt mixing provides insufficient shear force to break down GNP agglomerates and homogeneously disperse the platelets [82]. Yu et al. argued that the high percolation threshold of melt blended composites might be primarily due to high polymer melt viscosity that prevents the conductive fillers from forming a percolated network [24]. Additionally, polymer nanocomposites prepared through melt blending tend to agglomerate instead of becoming sufficiently dispersed particles [83], which suggests poor polymer-filler interfacial interaction during melt blending. Thus, some prior studies [84], [85] have utilized ultrasonic-assisted melt extrusion with PP/CB, PP/CNT, and PP/GNP to break apart agglomerates. However, this modified melt extruder configuration has short sonication times (of seconds compared to minutes for solvent sonication), thus resulting in minimal improvement in electrical conductivity.

1.3.2 Solution blending

Solvent blending is much more efficient than melt mixing [79]. This is because melt blending only results in good macroscopic dispersion, but with poor microscopic dispersion and poor exfoliation of carbonaceous fillers such as graphene due to the high viscosity of many polymer matrices [13]. Sonication in organic solvents is another

plausible route to graphene production. First, using a suitable solvent is a necessary prerequisite to help ensure more uniform microscopic dispersion of the fillers in the solvent. Second, ultrasonic waves generate pressure waves to break up filler agglomerates [38]. The sonication energy serves two purposes:

(i) shear force from the pressure helps to separate larger flakes and exfoliate individual graphene platelets apart by overcoming the binding energy among the graphene nanosheets [86]

(ii) cavitation and sonication energy can lead to the formation of micro-jets and shockwaves, which helps to achieve finer nanoscopic dispersion of graphene at higher filler loading [87]

However, ultrasonication does have many disadvantages, which may include low yields, a large energy requirement, and use of toxic solvents [88]. Since the ultrasonication process involves intense energy input over an extended period of time, this can result in localised structural and topological defects to graphene structure [40], as well as reducing the aspect ratio of graphene [89], all of which can drastically affect the mechanical and thermal properties of graphene. Moreover, one study found that the initial breakup of large CNT agglomerates is dependent on the sonication power, while the overall quality of the microscopic dispersion is more dependent on the cumulative energy input [32]. Thus, enhancing the effect of ultrasonication can improve the dispersion and exfoliation of carbonaceous fillers, at the risk of fragmentation and reduction in aspect ratio.

Dispersion of graphene fillers in solution with the aid of ultrasound can result in very few (less than 5) layers of graphene and small quantities of monolayer graphene [90]. For example, mixing GNP and polyetherimide in the presence of a solvent that can dissolve both the filler and the polymer allows the polymer chains to move freely and permeate into graphene sheets, thus preventing exfoliated graphene sheets from restacking [91]. Less agglomeration means a greater number of GNP particles able to be dispersed, thus available to form a conductive network. There are many research studies

on the dispersibility and solubility of various graphene-based fillers in different solvents [92].

However, quite often, it's not possible to dissolve both the GNP fillers and the polymer matrix. For example, solvents such as isopropanol can only disperse GNP but not polypropylene. This severely limits the applicability of the solvent blending approach. To address this problem, Kalaitzidou and co-workers proposed a novel method of 'coating' PP powder with GNP [82]. In this method, GNP flakes are dissolved and exfoliated through sonication in the presence of isopropanol, which is capable of dissolving GNP but not PP. Afterwards, non-dissolved PP powder is added to GNP-isopropanol suspension and mixed together via mechanical stirring. Thus, instead of dissolving the PP matrix, it is possible to simply 'coat' and deposit exfoliated graphene flakes onto the surface of non-dissolved PP particles. This method has proven to be very effective in prior studies [82], [91], [93], [94] because:

(i) dispersing GNP under ultrasonication helps to break down GNP agglomerates
(ii) exfoliated GNP particles are not taken out of solution and dried, which prevents restacking of exfoliated GNP fillers [17]
(iii) solution mixing helps to ensure excellent initial dispersion/coverage of PP particles before further processing. However, for injection molding and microinjection molding, further melt compounding is unavoidable to avoid screw slippage and ensure easy processability [62].
(iv) It is important to note that using a solvent that can dissolve PP, but not GNP, failed to produce good results due to poor dispersion and exfoliation of GNP [95].

PP powder can be obtained from suppliers, but it can also be prepared from pellets [96] or cryogenically milled. This technique has been attempted on other polymer matrices such as polyetherimide [91], polyvinyl chloride, and ultrahigh-molecular-weight polyethylene [97]. Moreover, better interfacial bonding can be achieved by the reduction in PP particle size due to a greater surface area. Nonetheless, it is still not optimal for two reasons. First, the solvent used (i.e., DMF and isopropanol) is usually optimized towards

the exfoliation of GNP sheets but cannot dissolve PP. A dual solvent at a specific ratio, such as *p*-Xylene:DMF, can be used to dissolve both PP and GNP simultaneously [98]. Second, extended duration of ultrasonication might damage graphene sheets and reduce the GNP particle size, resulting in greater amount of GNP intersheet junctions and greater contact resistance, thus higher electrical resistivity [99].

After precoating and melt compounding, it is possible to further mill the resulting composite down to micron size. Size reduction makes it more likely for GNP particles that are encapsulated in the polymer matrix to be exposed to the surface, thus more likely to be connected to other exposed GNP particles in subsequent molding [91]. In this case, the GNP particles would be less likely to be trapped in the crystalline regions of the polymer matrix, where they would not be part of conductive pathways [24]. Moreover, solid state ball milling and shear pulverization also provides sufficient shear force to break apart GNP aggregates to ensure more homogeneously GNP coating [93].

In situ polymerization

In situ polymerization involves adding graphene during the polymerization of the monomer to improve the dispersion of graphene [100]. Using this technique, Huang et al. reported uniform dispersion of graphene oxide (GO) in a PP host matrix, which exhibited high electrical conductivity of 0.3 S m^{-1} at 4.9 wt% GO concentration [101]. Milani et al. found that PP/graphene composites prepared by in situ metallocene polymerization most likely favored the growth of polymeric chains around the graphene sheets and facilitated its overall dispersion by preventing agglomeration of fillers. However, this also caused graphene nanosheets to be encapsulated by the polymer matrix, which prevented direct inter-particle contact and decreased the electrical conductivity despite improved dispersion [102].

1.3.3 Electrochemical Exfoliation

The principle behind electrochemical chemical approaches is to use an electrolytic solution for the expansion and exfoliation of graphite sheets [103]. Anionic

electrochemical exfoliation also works through the oxidative exfoliation of bulk graphite into GO, followed by chemical reduction into reduced graphene oxide (rGO) sheets [104]. The anions also function as surfactants to prevent restacking of graphene layers and facilitate dispersion of graphene sheets [105]. The exfoliation of graphite using anionic electrochemical exfoliation is shown in Figure 5 below. Su et al. showed that this method can produce high-quality graphene sheets, with a lateral diameter of several to 30 μm, which helps to reduce inter-sheet junctions, thus increasing nanosheet conductivity [99]. It is a viable method that can produce graphene flakes of less than 5 nm in thickness, with 5% of it being monolayer graphene [57]. Another study showed ~85% of flakes having merely 1–3 layers [105].

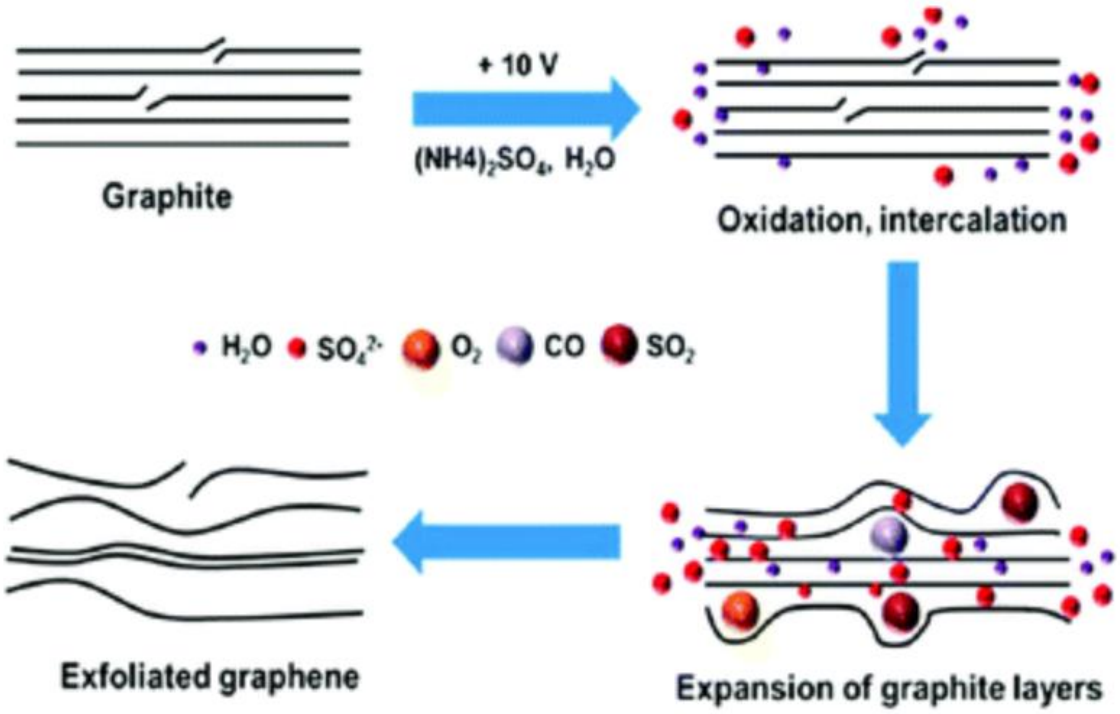

Figure 5: Illustration of electrochemical exfoliation through anionic intercalation, explained by Parvez et al. [105]

Generally speaking, the anionic method is more common than the cationic method, and it usually leads to good exfoliation of graphene flakes. However, this method tends to result in oxidized or functionalized graphene sheets due to the chemicals

involved [106]. This is a problem because these oxygen-based functional groups reduce graphene's electronic conductivity, which cannot be completely restored upon further chemical reduction, thereby losing some of the inherent advantages of pristine monolayer graphene such as high electrical and thermal conductivities [107]. On the other hand, cationic exfoliation avoids the production of oxidized sheets, but very few papers, including the most recent work by Cooper and co-workers, managed to form few layers in graphene flakes (2 nm thickness) through cationic exfoliation; although, the flake diameters are very small at around 100–200 nm [108].

1.3.4 Chemical Modifications

Compatibilizer:

Even though solvent mixing results in excellent dispersion [79], heat drying processing after solution blending might induce some restacking of GNP platelets [17]. Additionally, further processing such as melt compounding and injection molding might result in severe re-agglomeration that negates excellent dispersion and exfoliation of GNP fillers [109]. Nanoparticles with a large surface-to-volume ratio tend to agglomerate into clusters that are detrimental to the composite properties, and this problem can be addressed by adding compatibilizer to the nanocomposite to prevent agglomeration of GNP fillers. For example, one study demonstrated that pyrene-functionalized maleic anhydride-grafted polypropylene (g-MA-PP) can prevent stacking of exfoliated GNP and improve the compatibility of PP and GNP [98]. Using interfacial compatibilizer can help to facilitate the dispersion and prevent the agglomeration of the graphene-like flakes [110], [111].

Graphene Oxide:

Graphene oxide (GO) is a derivative of graphene-based materials. Chemical exfoliation of graphene, such as the Modified Hummers' Method, involves oxidizing graphite into graphite oxide, followed by exfoliation and reduction into reduced graphene oxide (rGO). This is a commonly used process because graphene oxide (GO) can be easily functionalized to improve exfoliation and dispersion [106]. The principal

advantage of utilizing GO is the ability to produce 90% monolayer GO sheets, but at the cost of highly oxidized graphene sheets and an extremely time-consuming process of repeated centrifugation [112]. Another advantage is that it provides a stronger interface with the polymer relative to unfunctionalized pristine graphene, with much less aggregation than most other graphene systems; this gives it a high level of mechanical reinforcement with relatively low optimal loadings [57].

Since GO is electrically insulating and thermally unstable, it is often necessary to reduce GO to remove its functional group to restore its electrical and thermal properties. However, the oxidation process when producing GO can severely damage the honeycomb lattices of graphene, resulting in significant and irreversible damage to graphene's electrical properties [99], [113]. More specifically, the process of reducing GO back to ordinary graphene is unable to fully recover the damage to graphene's structures, thus resulting in inferior mechanical and electrical properties compared to mechanically exfoliated pristine graphene sheets [44]. Hence, the product, reduced graphene oxide (rGO), nonetheless exhibits many defects compared to pristine graphene, and complete reduction of graphene oxide rarely occurs [53].

Surface Modification:

Chemical functionalization of the fillers can be an effective method for enhancing the interfacial interactions between the fillers and the polymer matrix. This can be accomplished by methods such as oxidation, physical adsorption, and grafting [114]. For example, CNT [115] and GNP [116] can be modified to increase the adhesion between the polymer and filler. This will help to maintain filler dispersion while forcing the filler to selectively aggregate at the matrix-filler interface, thus forming filler-rich regions and creating sufficiently dense conductive pathways. However, the effectiveness of functionalized graphene in preventing the agglomeration of GNP particles is disputed [117].

1.4 Microinjection Molding

Small scale injection molding is becoming an important technology to fabricate miniature products and components, especially in microelectromechanical systems (MEMS) [1], [3]. Moreover, Fred Chiou [2] summarized the following advantages of using microinjection molding:

- Cost-effectiveness for mass production process
- Can be used with a wide range of thermoplastics
- Good process control, automation, and accurate part replication
- Relatively low-maintenance costs of capital equipment
- Large amount of information available from conventional injection molding.

In microinjection molding, the polymer is loaded into a hopper, melted, and rapidly injected into the mold cavity under high pressure. The material is then cooled down into the mold shape and ejected. Polymer composites are often used as molding materials due to their weight advantage, processability, and resistance of wear and corrosion, with thermoplastic polymers being most widely used [4]. The figure below shows a simplified diagram of the injection molding process, where an injection piston pushes the polymer melt into the mold cavity.

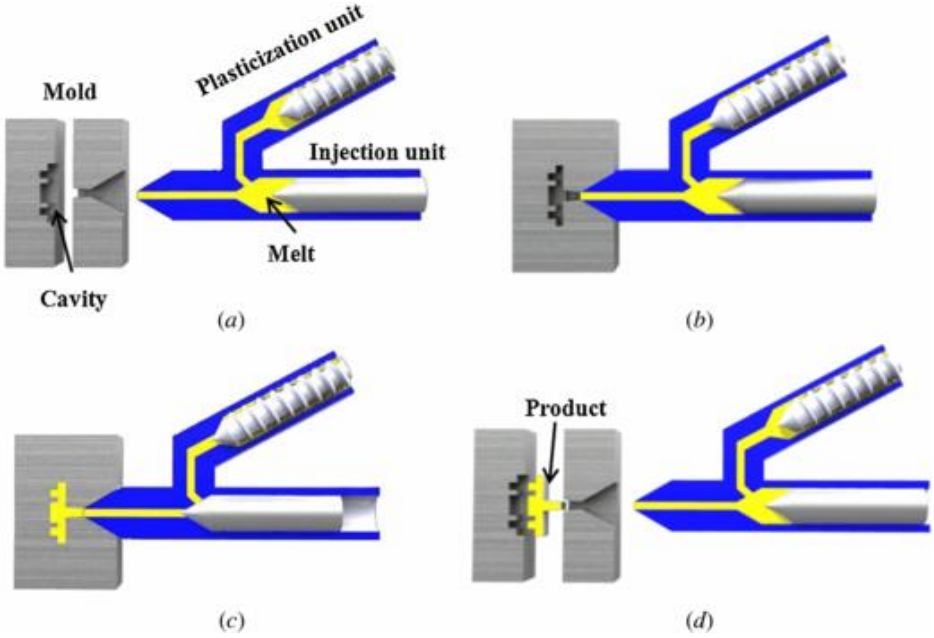

Figure 6: The various stages of the μIM (with separate plasticization and injection units) process. Herein: (a) plasticization of polymer (b) mold closing (c) injection, packing, and cooling, and (d) demolding and re-plasticization [1].

However, μIM is not merely a scaling down of conventional injection molding (CIM). The polymer melt will experience extremely high shearing effects in μIM since it involves higher injection velocities and higher molding temperatures [6]. Thus, it is anticipated that very high shear rates would generate severe shear stress fields, which cause fillers to favorably align in the flow direction. Moreover, strong shear forces and friction forces that act on the polymer matrices can damage molecular chains, which helps to explain why mechanical and thermal characteristics of microparts are inferior to the feed blend [118]. Factors such as higher temperature can also lead to polypropylene chain degradation [119]. Additionally, previously negligible factors in CIM such as microscale rheological flow behavior, wall slip, and surface tension can significantly influence the material properties of microparts [3], [7]. The extremely high pressure in μIM also results in non-negligible effects of melt compressibility [8] and preferred orientation of macromolecular chains along the flow direction. Moreover, the rapid cooling of the material during the contact with mold wall partially contributes to the ‘skin-core’ structures in CIM. Reduced part thickness and higher aspect ratio of μIM

microparts increases shear deformation and cooling rates [9]; temperature is one of the main factors that determines the quality and properties of μIM microparts [3].

Effect of Mold Geometry

Zhou et al. [19] studied the properties of microinjection molded nanocomposites using a step-mold, which produced microparts with three different thickness – thick, middle, and slim – as shown in Figure 7b below. However, one question is whether the sudden decrease in micropart thickness (i.e., the 'step' feature) affected the observed electrical conductivity. Hence, the proposed research involves analyzing the thermal, electrical, and morphological properties of a micropart of uniform thickness dimensions (plaque micropart), as shown in Figure 6a. The purpose of producing simple rectangular-shaped plaque microparts, as shown in Figure 7d, is to establish baseline electrical conductivities of various polymer composites without having to consider any geometrical effects. Additionally, the material combinations and process conditions used in this thesis are identical to that Zhou et al. for consistency purposes.

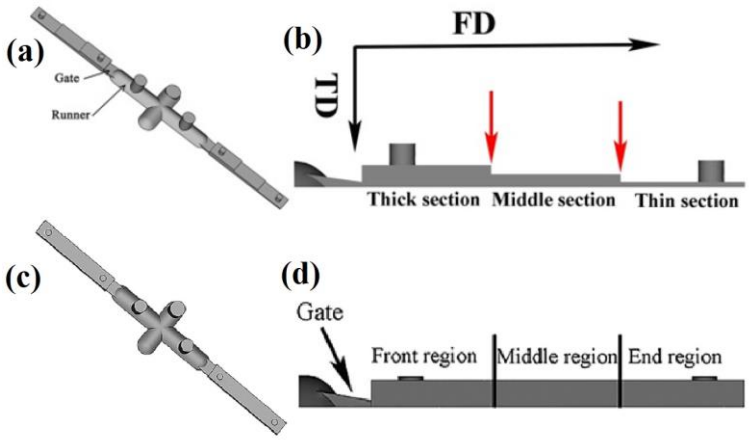

Figure 7: The original step microparts (top) and the constant-thickness plaque microparts (bottom) adapted from previous studies [19]. Herein: (a, c) 3D view of a finished micropart (b, d) micropart divided into three sections for easy referencing and characterization.

There are some literature sources that suggest that mold geometry is not the most dominant factor. White and Dee studied flow visualization for the injection molding of

polymer melt into a rectangular mold, which suggests that more fountain flow is to be expected for the rectangular micropart than the step micropart. [120]. Chu suggested that injection speed is the most important factor, more so than the shape of the mold cavity, because the choice of injection speed directly influences melt temperature, injection and mold cavity pressure [121]. Moreover, using a mold insert might also cause variations in cooling conditions, which also needs to be accounted for [122].

High Shear Conditions:

Due to the extremely high shearing effects in μIM [6], it is possible for shear deformation to result in a conductive network of interconnected secondary agglomerates [33], [123]. For this to occur, the initial primary agglomerates must be broken up and well dispersed in the polymer matrix in the mixing stage. In further processing steps, such as CIM and μIM, the filler network can be formed by secondary agglomerates, which is shown in Figure 8. Moreover, one study found that polypropylene chain degradation is primarily caused by chain scission that is promoted by a combination of factors including chain entanglements, temperature, shear rate, and viscosity [119], all of which are exacerbated by the processing conditions in microinjection molding.

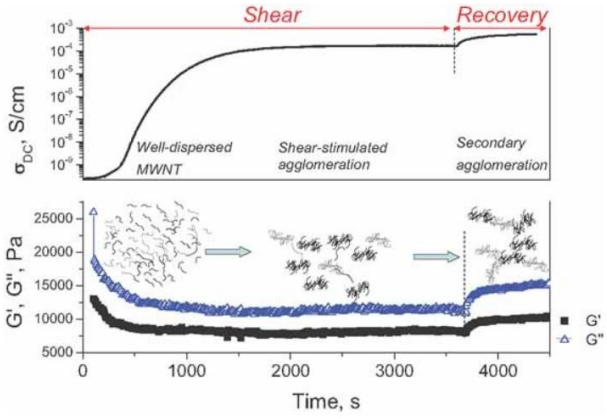

Figure 8: Illustration of the effect of steady state shear applied to an initially non-conductive composite with initially well-dispersed nanotubes [124]

Future Applications:

In the future, the μIM system could become the compromise solution between household 3D printers and industrial production lines because μIM offers greater precision and production volume compared to 3D printers. [125] Injection molding for internal biological application is also being explored; one example is producing biodegradable implants for medical purposes [126]. Using existing μIM technology for producing both micro and nano-scale features is also being investigated. [127] Specific studies regarding the effect of micro-cavity dimensions on the material properties of microparts have been conducted [128]. However, one challenge with μIM is that producing mold cavities with micro features with CNC machining and lithography can be very expensive, while also requiring complex technical capabilities [129]. Another challenge is a complex quality assurance system is often required to ensure that high precision micro features are guaranteed [4].

1.5 Characterization of microinjection molded microparts

1.5.1 Electrical Conductivity

The conductivity of a PP-filler composite system derives from the formation of a conductive network by the fillers within the PP polymer matrix [130]. The surface resistivity and bulk resistivity of thin sheets can be calculated from measured resistance using the 4-probe method [131]. Larger samples can be measured using a simple 2-probe approach to obtain bulk conductivity [12].

There is a significant amount of research on enhancing the electrical conductivity of polymer composites by incorporating carbon-based fillers at various filler loadings and with different manufacturing techniques [132]. Factors such as filler geometry (i.e., aspect ratio), concentration, directional alignment, and percolation threshold may all play an important role in the conductivity of the filled polymer composites [133]. Moreover, techniques such as surface treatment can help to improve the interfacial interaction between CNT and polymer matrix to improve electrical conductivity [134].

1.5.2 Morphology

Polymer melts, such as polypropylene (PP), behave as a shear thinning non-Newtonian fluid, where the fluid viscosity decreases with increasing shear rate. At low shear rates, PP melt will show a constant viscosity value. At and above a critical shear rate, there will be a significant drop in viscosity, which is the shear thinning region. At high shear rates, which is characteristic of the μIM process, carbon fillers in PP-based composite materials will be preferentially align along the flow direction, resulting in the rearrangement of filler dispersion. More specifically, CNT fillers tend to agglomerate into cylinder-like nanotube bundles, GNP fillers might restack into graphitic flakes, and spherical CB particles are likely to form small 'grape'-like aggregates [13]. Most importantly, excess agglomeration caused by high-shear conditions of the μIM process might impede the efficiency of which carbon fillers can disperse and form a conductive network, thus elevating the percolation threshold.

1.5.3 Thermal Stability

The thermal stability of polymer-carbon composites can be measured through thermogravimetric analysis (TGA), where the change in mass of a polymer is measured as a function of temperature or time in a controlled atmosphere. This method can yield data such as decomposition temperature (T_d, taken at 5% weight loss), maximum decomposition temperature (T_{max}, peak of 1st order derivative weight loss), and percentage remaining as char at the end of the heating cycle (R_{560}, subscript denotes the end temperature of the heating cycle) [135]. Different types of purge gas may be used, such as inert (nitrogen, argon, or helium), oxidizing (air, oxygen), or reducing gases (forming gas), with a heating rate around 5–20°C/min; different testing conditions may also play a role in the thermal stability results [83].

The addition of GNP to polymer matrix has shown to improve the thermal stability of the composites, with one study reported an increase of T_d from 259°C to 295°C at 15 wt% graphene loading [95]. There are several mechanisms that have been proposed to explain this observation. First, GNP fillers can act as heat sinks to withdraw some heat from the polymer matrix, and thus prevent the accumulation of heat within the

polymer and delay oxidation at the early stage of thermal degradation [136]. Second, well-dispersed GNP fillers can serve as efficient mass transfer barriers against the volatile pyrolyzed products, hindering the movement of oxygen and volatile products throughout the material [137]. But the addition of GNP fillers will result in decrease in the amount of phase changing material, which in turn reduces latent heat storage capacity [138].

1.5.4 Crystallization

Differential Scanning Calorimetry (DSC) is a technique that can be used to measure the heat flow in or out of a material, as a function of time or temperature. The crystallization behavior of the polymer can be quantified by the heat of fusion and heat of crystallization of the polymer composite. Since the thermomechanical history can affect the properties of the samples, each sample was scanned three times. The first cycle (heating) is reflective of the thermomechanical history of the microparts due to melt compounding and the μIM process, which might have affected the micropart microstructure. The second cycle (crystallization) was for the purpose of analyzing the crystallization behavior, which might include some dissipation of the filler microstructure. The third cycle (heating) is measuring the material properties without much influence of melt mixing and μIM process.

There are studies that showed that the MWCNTs acted as α-nucleating agents in iPP [139]. Generally speaking, increased CNT loading may result in increased crystallization temperature (T_c) and percent crystallinity (X_c) of PP/CNT composites, thereby confirming the nucleating effect of CNT by increasing the number of nucleation sites [86]. One study argued that CNT is a strong α-nucleating agent, which can suppress nucleation of β-crystals and forced the material to exclusively yield α-crystals after reaching 2.5wt% CNT loading [140]. However, another study showed that, while a great number of studies testified the ability of CNT to promote the crystallization and the formation of α-PP crystals, which are the dominant crystal forms for iPP, CNT can also induce the formation of β-crystals [141].

Crystallization can affect the formation of conductive pathways by concentrating filler aggregates in the amorphous phase of polymer matrix. Yu et al. found that slower

crystal growth could help to push CB aggregates into amorphous regions of the PP matrix, where they are less likely to be trapped in crystalline regions where it could not participate in the formation of conductive pathways [24]. Similarly, GNP fillers have good nucleation ability. Achaby et al. [142] reported a 6°C increase in melting temperature (T_m) and 9°C increase in T_c at 3 wt% GNP loading. However, crystals can develop on the surface and envelop the GNP filler; this will increase contact resistance and reduce the number of filler particles available to form continuous conductive network [62]. Thus, one approach is to deliberately influence fillers to agglomerate at an interface, such as the 'coating' method [143].

Slower cooling rate is also favorable towards the formation of effective conductive pathways, which is shown in Figure 9, by promoting the growth of larger crystal sizes of a few microns, thus more effectively displacing CNT fillers from the crystallized region to the amorphous phase; larger crystal size is a more dominant factor over % crystallinity structure [144]. Similarly, reducing the CNT nucleation effect on PP crystallization and forming large crystallites (shown as a wider crystallization peak on the DSC thermographs) will allow more CNT to migrate to the amorphous phase to selectively develop a distributed network structure [144]. Moreover, the degree of crystallinity is independent of GNP flake diameter [57].

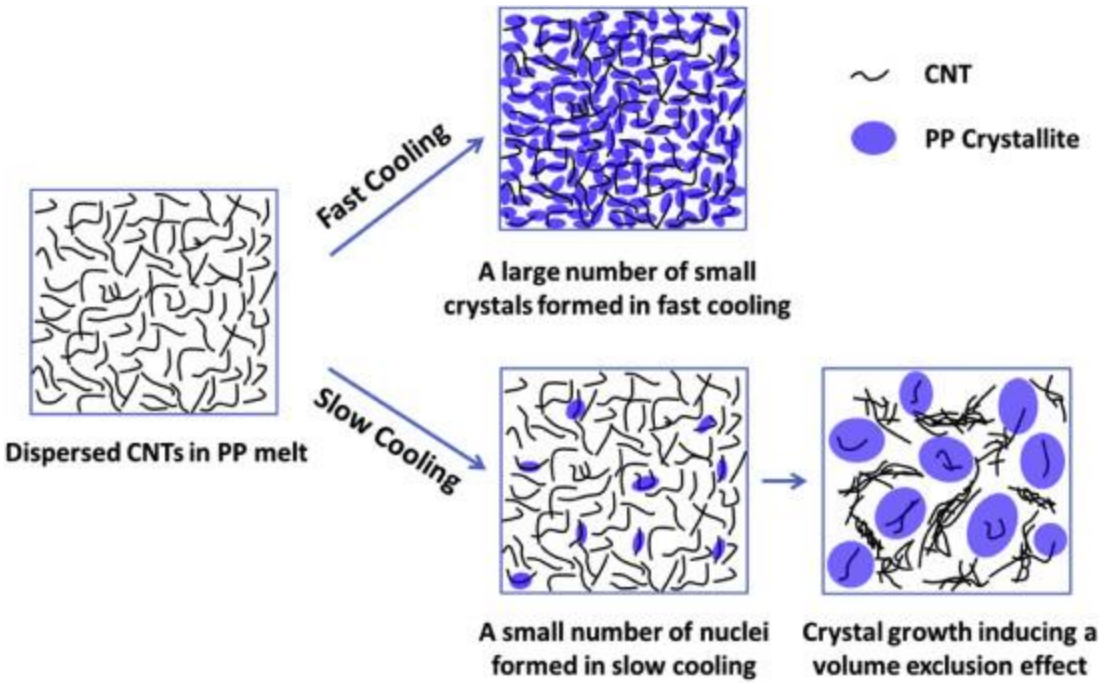

Figure 9: Effect of slower cooling rate on the crystallization behavior of compression molded PP/CNT composites [144].

1.5.5 Rheology

There are several studies that reported a significantly lower rheological percolation threshold than electrical percolation threshold for CNT-based composite materials [84], [85], [145]–[147]. The difference between the electrical and rheological percolation thresholds is mainly attributed to different stages of nanotube network required. For example, Du et al. reported the rheological threshold at 0.12 wt% and electrical threshold at 0.39 wt% in a SWCNT/PMMA system [147]. Hu et al. found the rheological and electrical threshold for a MWCNT/PET system to be 0.6 wt% and 0.9 wt%, respectively [145]. This discrepancy can be explained by the smaller nanotube−nanotube distance required for electrical conductivity as compared to that required to impede polymer mobility (i.e., rheological percolation) [147]. The CNTs need to be very close, but do not need to come into direct physical contact, to achieve electron tunneling/hopping process [148]. The nanotube–nanotube distance required for rheological percolation (to restrict polymer chain mobility) is longer than that for electrical percolation, thus fewer nanotubes are needed to achieve rheological percolation

than electrical percolation [149]. The ‘physical network’ formed by entangled polymer chains impede polymer chain movement, thus increasing viscosity [145].

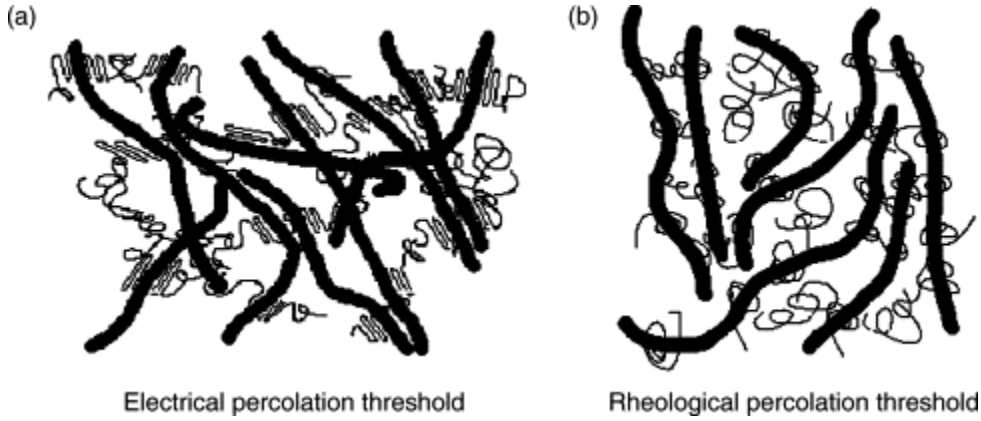

Figure 10: Illustration of electrical percolation threshold (a) and rheological percolation threshold (b) in PET/MWNT nanocomposites. The thick lines stand for MWCNT, and the thin ones for PET chains [145]

Similarly, the addition of GNPs in a polymer matrix will increase the melt viscosity, which is related to the formation of the GNP network in the polymer melt which strongly depends on the aspect ratio and the degree of exfoliation of GNP. Compared with carbon black, carbon nanofibers and carbon nanotubes, GNP-filled polymer nanocomposites have the lowest melt viscosity in a certain range of filler loadings, indicating better processibility [110]. This associates with the ability of different nanostructures in various polymers to form network structures that could constrain the motions of polymer chains. A possible reason for the lower viscosity is that the 2D structure of GNP might also act as a solid lubricant [150]. Moreover, at lower filler loading, factors such as better dispersion, smaller particle size, and higher degree of exfoliation will result in greater filler surface area and encourage stronger interfacial bonding. Thus, better processing methods might lead to more efficient GNP networks, and consequently, higher storage and loss modulus and more obvious shear thinning behavior [151].

Chapter 2

2 Experimental Methodology

Materials, equipment, and analysis techniques used in this thesis are detailed in this section.

2.1 Materials

Polypropylene

Isotactic polypropylene in pellet form (PP, Product number: 427888, average Mw: ~250,000) was purchased from Sigma Aldrich. The material has a density of 0.9 g/cm^3 and a melt flow index of 12 g/10 min (230°C @ 2.16 kg load).

Isotactic polypropylene in powder form (PP, SM 6100, average Mw: ~264,000) was acquired from the Shell Oil Company. The material has a density of 0.9 g/cm^3 and a melt flow index of 12 g/10 min (230°C @ 2.16 kg load).

Carbonaceous Fillers

Table 1: Properties of Carbonaceous Fillers

Filler	Manufacturer	Grade	Density [g/cm^3]	Surface area [m^2/g]
CB	Akzo Nobel Polymer Chemicals LLC. (Chicago, IL, USA)	Ketjenblack® EC-600JD	1.80	~1400
CNT	Hyperion Catalysis International (Cambridge, MA, USA)	MB3020-01	1.75	178
GNP	XG Sciences Inc. (Lansing, MI, USA)	xGnP® Grade M	2.2	120 ~ 150

Nanocomposites with CNT were produced through the melt dilution of PP/CNT masterbatch obtained from Hyperion Catalysis International. According to the manufacturer, its proprietary nanotubes (FIBRILTM) were vapor grown with a length over 10 μm and an outside diameter about 10 nm. The material's density and surface area were

found in literature sources [152], [153]. Relevant information about the EC-600JD CB was obtained from data sheet provided by the supplier and listed in the table above. Graphene nanoplatelets were purchased from XG Science Inc. (Lansing, MI). Based on data obtained from the manufacturer, the grade M15 particles have an average thickness of approximately 6 to 8 nm, a typical surface area of 120 to 150 m^2/g, and an average particle diameter of 15 μm.

2.2 Preparation of Materials

2.2.1 For PP/CNT and PP/CB samples in Chapter 3.1:

A Brabender twin-screw batch mixer (C.W. Brabender Instruments, Inc., South Hackensack, NJ, USA) was used to mix the PP and carbon fillers (CB and CNT separately) at 50 rpm and 190°C for 10 min. Samples with concentrations of CB and CNT at 1, 2, 3, 5, 7, 10, and 15wt% were prepared. PP/CNT composites were obtained from the melt dilution of PP/CNT masterbatch. PP/CB composites were obtained from direct melt mixing of PP pellets with CB. The blended materials were pulverized into pellet-sized chunks using a commercial blender, then loaded into a microinjection molding system (μIM, Microsystem 50, Wittmann Battenfeld) to produce microparts for testing. The following nomenclature was adopted for easier identification of samples:

- PP/CB# refers to PP and CB composites, where # denotes the weight percentage of CB fillers. T (thick, 0.83mm) or M (middle, 0.50mm) can be appended at the end of the nomenclature to indicate the micropart's thickness, and the absence of T/M indicates not-micromolded composite materials (feed blend). For example, PP/CB2T indicate a "thick" micropart with a thickness of 0.83mm produced from PP/CB composites with 2 wt% CB filler loading.

- PP/CNT# refers to PP and CNT composites, where # denotes the weight percentage of CNT fillers. T (thick, 0.83mm) or M (middle, 0.50mm) can be appended at the end of the sample name to indicate the micropart's thickness. The absence of T/M indicates feed blend. For example, PP/CNT5M indicate

microparts with a thickness of 0.50mm produced from PP/CNT composites with 5 wt% CNT filler loading.

2.2.2 For PP/(CNT:CB) hybrid samples in Chapter 3.2:

The polymer nanocomposites with various carbon filler concentrations (3, 5, and 10 wt%) at various weight ratios of CNT:CB (100:0, 30:70, 50:50, 70:30, 0:100) were prepared by melt blending in a similar fashion as described in chapter 2.2.1. For example, PP/(CNT30:CB70)3M denotes:

- The microparts are 0.50mm thick
- The total filler weight is 3wt%, of which 0.9wt% is CNT (obtained from melt dilution of PP/CNT masterbatch) and 2.1wt% is CB
- Absence of T/M indicates not-micromolded feed blend

2.2.3 For PP/GNP samples in Chapter 3.3:

Kalaitzidou and co-workers proposed a method of precoating PP powder with exfoliated graphene nanoplatelets (GNP) by sonication in the presence of isopropanol to complete cover PP powders with GNP [82]. This process was modified and briefly described below:

- GNP was added to 1L of isopropyl alcohol, which was purchased from Sigma Aldrich (Oakville, Canada). Then, the obtained mixture was ultrasonicated for 1 hour to yield uniformly dispersed GNP solution
- A certain amount of PP powders was slowly added and stirred at high speed for 30 min, followed by another 1 h of sonication; after that, solvent was removed through vacuum filtration. Any remaining solvent was evaporated at room temperature
- The word “premixed” and “precoated” are used to describe this process of solvent-based premixing of PP and GNP

The study in Section 3.3 of this thesis compares the properties of μIM microparts (all 0.83mm thick) prepared through three different methods: (i) direct melt mixing PP of pellets with GNP fillers (ii) direct melt mixing PP of powders with GNP fillers (iii) precoating of PP powder and GNP fillers through solvent-based ultrasonication, but

subsequent melt compounding is required for easy processability in injection molding systems [62].

All samples from all three methods were melt blended for easy processing in the μIM system. A Brabender twin-screw batch mixer was used to melt blend PP and GNP fillers at 50 rpm and 190°C for 10 min. The concentrations of GNP filler were at 3, 5, 7.5, 10, 12.5, and 15wt%. The blended materials were pulverized into pellet-sized chunks using a commercial blender, then loaded into a microinjection molding system (μIM, Microsystem 50, Wittmann Battenfeld) to produce microparts for testing. The following nomenclature was adopted for easier identification of samples:

- Pellet-PP/GNP3 refers to composites prepared by mixing PP pellet and GNP with 3wt% total filler loading
- Powder-PP/GNP5 indicates composites prepared from PP powder and GNP at 5wt% filler loading
- The word “blend” refers to not-micromolded composite materials (feed blend)

2.3 Preparation of Microparts

The preparation of a micropart using the Battenfeld microinjection molding system can be summarized as the following four steps. First, the raw material is loaded to a hopper, which is then fed into the extruder screw. Second, the extruder screw melts the polymer – at the melt temperature – and pushes the exact amount of material into the metering chamber. Third, the injection piston pushes molten polymer from the metering chamber into the mold cavity. Lastly, the mold is cooled down, and the microparts are automatically ejected from the mold cavity.

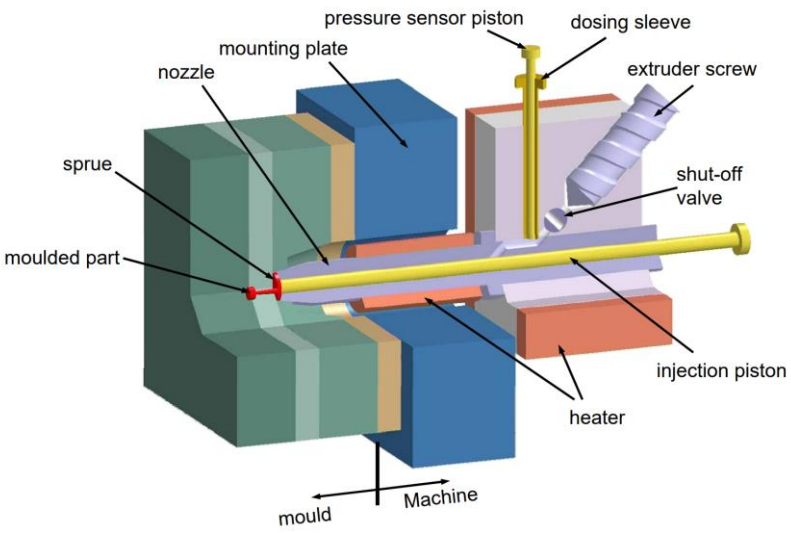

Figure 11: Internal Schematics of the micro-injection-molding system. Taken from: http://www.battenfeld.ru/fileadmin/templates/docs/imm/microsystem_presentation.pdf

The mold cavity was specifically designed to accommodate microparts of varying thickness. More specifically, mold inserts can be used to adjust the thickness of the microparts to either 0.83mm (thick), 0.50mm (medium), or 0.2mm (slim). The microparts were produced at a melt temperature of 260°C, mold temperature of 100°C, and injection speed of 300 mm/s.

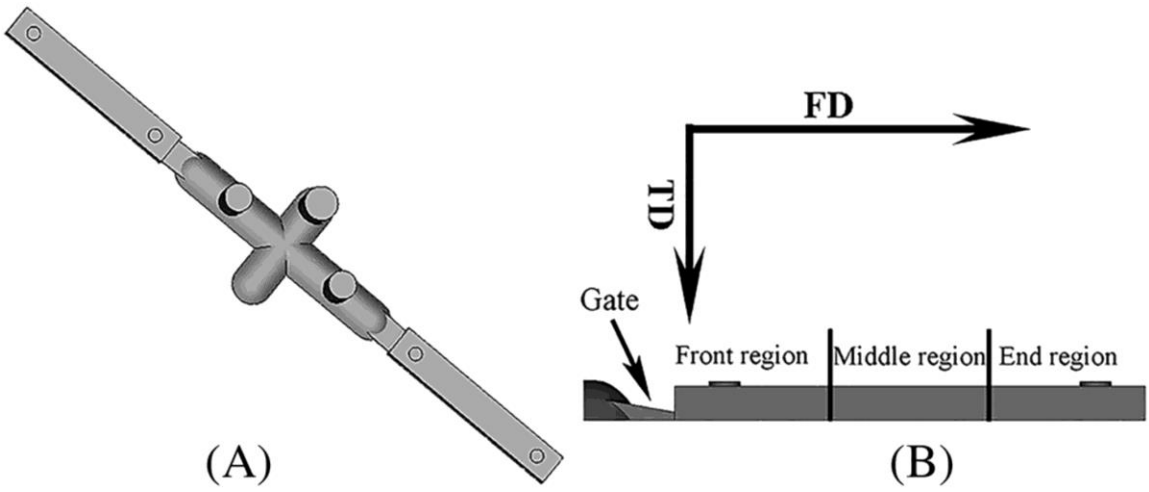

Figure 12: (a) 3D view of a finished micropart and (b) the micropart was divided into three sections, where the middle region was taken for various characterizations [154]

2.4 Characterization

2.4.1 Electrical Conductivity

The electrical conductivity (σ, S/cm) was determined using a two-probe method as follows. For each sample, the micropart was placed between two copper electrodes, and applied pressure to minimize the contact resistance between the electrodes and the surface area of the sample. A Keithley 6517B (Tektronix Inc., Beaverton, Oregon) electrometer was used to measure the direct current (DC) electrical resistance (R, Ω) along the melt flow direction (FD) and transverse direction (TD). Using the external dimensions of the micropart and the measured R value, the electrical conductivity (σ, S/cm) can be calculated as per Equation (1):

$$\sigma = \frac{1}{\rho} = \frac{L}{AR}$$

where, L (cm) is the distance between the measuring electrodes, R(Ω) is the electrical resistance, and A (cm^2) is the contact area between the electrodes and the sample. The average σ value, as calculated from five samples, was used. Moreover, the electrical percolation threshold (p_c) is achieved when the σ of polymer composites sharply increases, often by several orders of magnitude, due to the formation of continuous conductive pathways are formed from a sufficiently dense filler network. The σ at p_c is at least 10^{-10} S/cm or higher for microparts produced in this thesis.

2.4.2 Morphology

Finished microparts were observed using scanning electron microscopy (SEM). First, microparts of various material combinations were cryogenically fractured using liquid nitrogen towards the middle region of the (0.83mm) thick microparts in the TD, as shown in Figure 12(b). Second, the fractured microparts were subjected to chemical etching using a solution of 64.7wt% H_2SO_4, 32.3wt% H_3PO_4, and 3wt% of $KMnO_4$ for at least 7 h. Afterwards, microparts were rinsed using distilled water, 3wt% hydrogen peroxide, and acetone. [155] Third, the fractured surface was sputter coated with a thin layer of

platinum, and then observed using SEM for both the core and skin layers of the microparts.

2.4.3 Thermogravimetric Analysis (TGA)

The thermal stability of each sample was determined by a thermogravimetric analyzer (TGA). Feed blends were used as-is without further processing, and samples from molded microparts were taken near the middle of the microparts. Tests were carried out under constant nitrogen flow and a heating rate of 10°C/min. The testing conditions for each sample are given in the following table.

Table 2: TGA Testing Conditions of Composites and Molded Samples

Section 3.1: PP/CB and PP/CNT	320 to 560°C	TG 209F1 Iris, Netzsch
Section 3.2: PP/(CB:CNT) Hybrid	240 to 600°C	TG 209F1 Iris, Netzsch

2.4.4 Differential Scanning Calorimetry (DSC)

The melting and crystallization behavior of pure PP and filler-containing PP composites were examined with a differential scanning calorimeter (DSC, Q200 and Q2000, TA Instruments) under nitrogen atmosphere with a gas flow rate of 50 mL/min. Feed blends were used as-is without further processing, and samples from molded microparts were taken near the middle region of the microparts.

The first cycle (melting) reflects the thermomechanical history of the microparts due to melt compounding and the μIM process. The second cycle (crystallization) was used to analyze the crystallization behavior. The third cycle (melting) reflects the material properties without much influence of previous thermomechanical history. In Sections 3.1 and 3.2, the samples were scanned from 30 to 200°C with a temperature increasing rate of 10°C/min (1st cycle), and then cooled down at a rate of 50°C/min to 30°C (second cycle), and finally scanned from 30 to 200°C at 10°C/min (3rd cycle). In Section 3.3, the samples were scanned from 30 to 230°C with a temperature increasing rate of 10°C/min,

and then cooled down at a rate of 10°C/min to 30°C, and finally scanned from 30 to 230°C at 10°C/min.

The melting temperature (T_m) was obtained from the heating cycle and the peak crystallization temperature (T_c) was obtained from the cooling cycle. The crystallinity (χ_c) was calculated with Equation (2):

$$\chi_c = \frac{\Delta H_m}{(1-w)\Delta H^{calc}} \qquad (2)$$

where ΔH_m is the melt enthalpy of isotactic PP, w is the weight fraction of GNP filler in PP, and ΔH^{calc} is the melting enthalpy for 100% crystalline PP, which is 207 J/g [156].

2.4.5 Melt Rheology

Melt rheology testing can be utilized to study the microstructure of filled PP composites. This test is mainly focused on the flow behavior, viscosity, and deformation of filler structure of the composite material. In Section 3.2 with PP/(CNT:CB) hybrid composites, the test was conducted using a rheometer (Bohlin Gemini 200, Malvern) with a parallel plate setup. The tests were performed within a frequency sweep from 0.01 to 100 Hz at 190°C.

3 Results and Discussion

3.1 Effect of Mold Geometry

Zhou et al. [19], [157] studied the properties of microinjection molded nanocomposites using a step-mold, which produced microparts with three different thickness – thick (0.83mm), middle (0.50mm), and slim(0.20mm). However, one question is whether if the sudden decrease in micropart thickness (i.e., the ‘step’ feature) affected the material properties of resultant CNT-filled and CB-filled microparts. In this section, simple rectangular shaped plaque microparts were produced using identical process conditions, materials, and experimental procedure as prior studies by Zhou et al. Afterwards, the electrical, thermal, and morphological properties of the plaque microparts were compared to the properties of step microparts to determine whether the ‘step’ feature resulted in significant changes to the material properties of the finished microparts.

3.1.1 Electrical conductivity

The electrical conductivity using a two-probe approach, and results for plaque-microparts were compared to the step-microparts used in past studies.

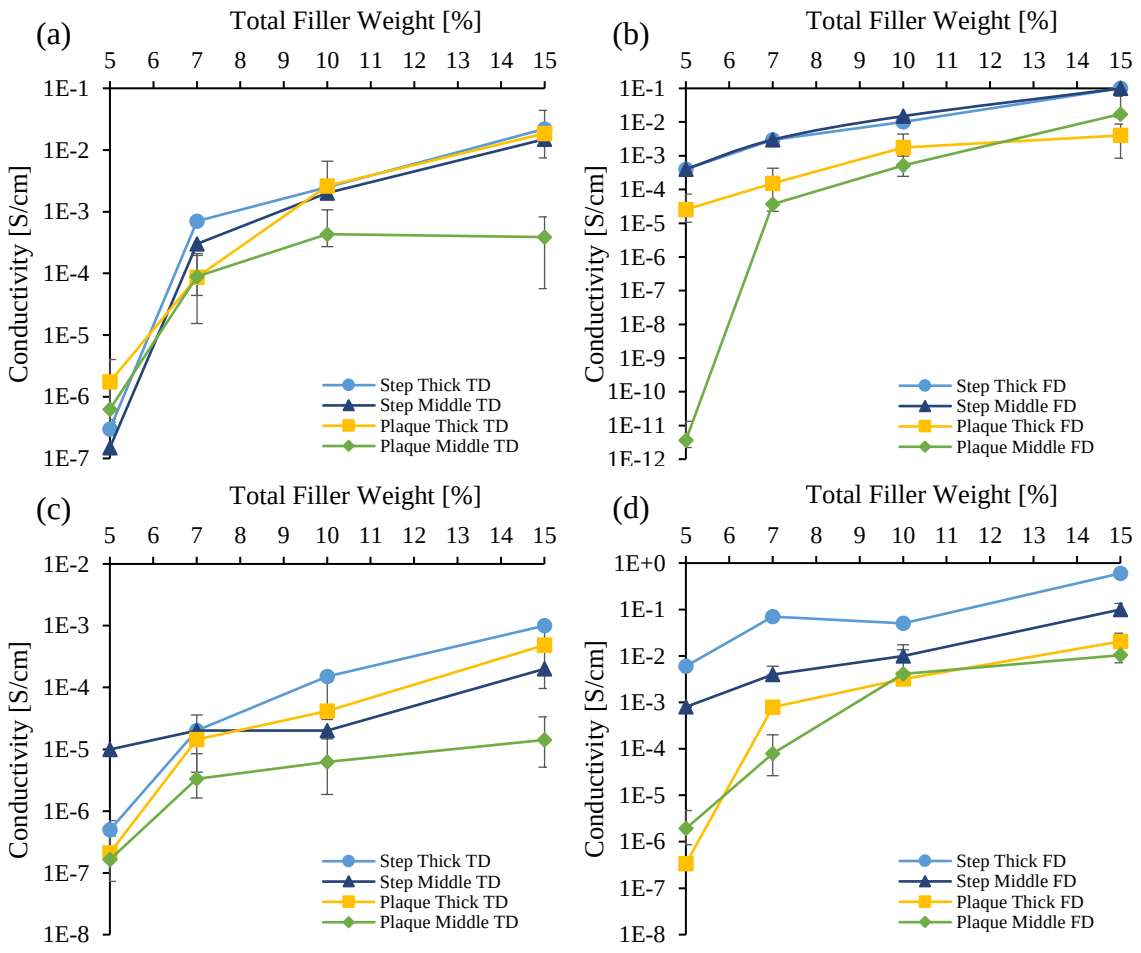

Figure 13: Comparison of the electrical conductivity (σ) between the plaque microparts and step microparts for (a) PP/CB TD (b) PP/CB FD (c) PP/CNT TD (d) PP/CNT FD. FD refers to the flow direction and TD denotes the transverse direction, which is perpendicular to the flow direction.

A comparison of σ of plaque microparts and step microparts is given in Figure 13. For both CB-based and CNT-based microparts, the σ values for step microparts were consistently higher than corresponding plaque microparts of the same thickness. For both PP/CB and PP/CNT microparts, this difference in σ is approximately one order of magnitude on average along the TD and two orders of magnitude along the FD direction.

There are several possible explanations for this. One factor is that at each thickness, step mold microparts are much shorter than plaque microparts. For example, the thick section (0.83mm) of a step micropart is only 5mm long, whereas a plaque micropart is 14.3mm

long. Thus, the difference in σ value might be different due to flow conditions and filler distribution at various distances away from the gate region. Wegrzyn et al. reported that the concentration of CNT fillers generally increases further away from the gate region, except in the area immediately adjacent to the runner due to disturbed polymer flow [158]. Hence, the shorter step microparts (i.e., the section is closer to the gate region) might have contained disproportionately high filler concentration, thus more likely to result in higher σ than plaque microparts with longer flowing distance. Additionally, since the abrupt decrease in mold thickness (i.e., the 'step' feature) can result substantial difference in filler distribution. For example, Zhou et al. [159] found that the number of CNT agglomerates found within different sections of the micropart decreased with thinner parts, which could be ascribed to the sudden and significant increase in shear rate brought by the 'step' feature. The abrupt change in mold geometry might also cause flow disturbance or entrap larger agglomerates.

Changes in micropart thickness had a smaller effect on the σ in CB-filled microparts in Figure 13 (a, b) compared to CNT-filled microparts in Figure 13 (c, d). Additionally, Figure 13 (c, d) showed there is less difference in σ between plaque vs step microparts at the same thickness for CNT-filled microparts. Since reducing thickness results in higher shear rate, this can also be attributed to CNT rod-like structure being more susceptible to sudden changes in shear rate and flow conditions caused by the 'step' feature [159].

3.1.2 Morphology

The morphology of PP/CB and PP/CNT plaque microparts was examined using a SEM microscope in both the core layer and skin layer. This was then compared to prior studies as well.

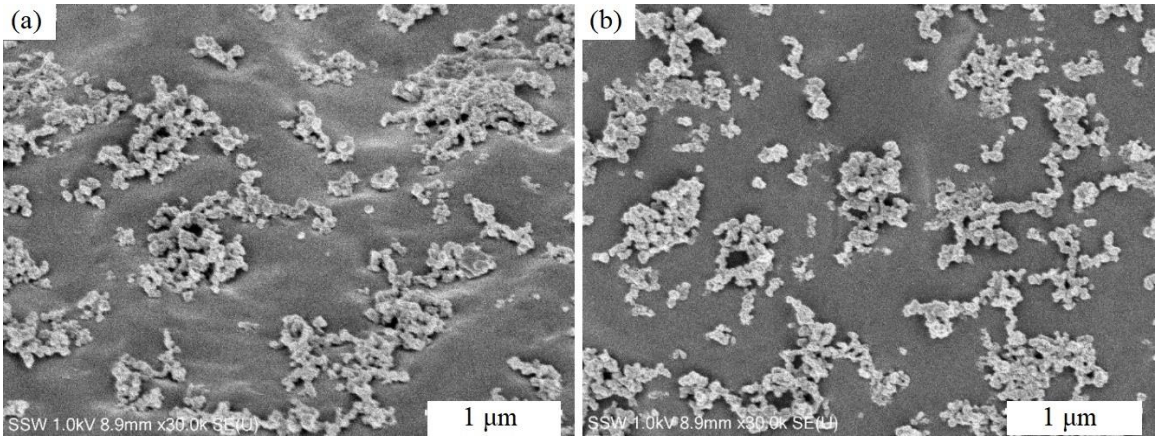

Figure 14: SEM images of the (a) skin layer (b) core layer of PP/CB2T micropart

SEM images of PP/CB 2 wt% in Figure 14 showed CB aggregates uniformly distributed in both the core layer and the skin layer, whereas a prior study by Zhou et al. using step microparts showed significant CB depletion in the shear layer. [19]

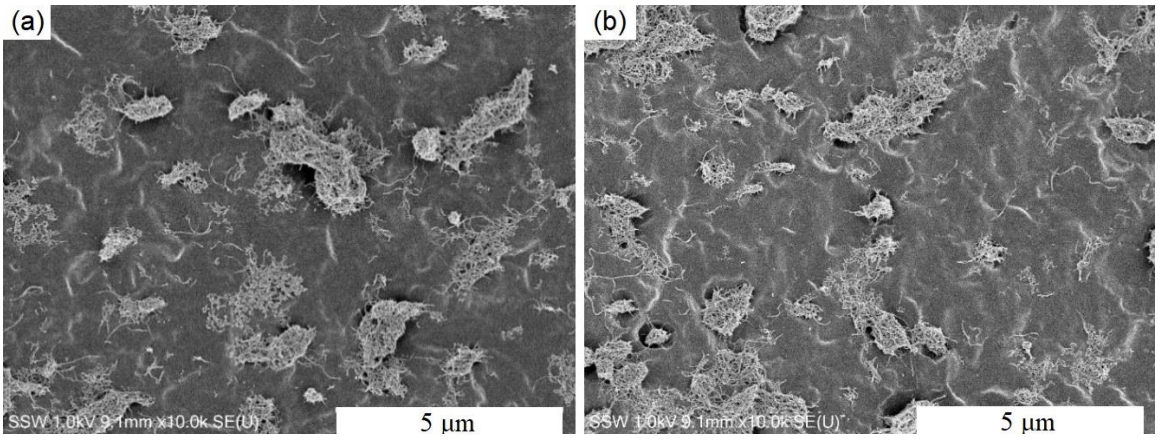

Figure 15: SEM images of the (a) skin layer (b) core layer of PP/CNT2T micropart

Figure 15 shows the SEM images of PP/CNT 2 wt% plaque microparts in the shear layer and core layer. Results revealed that CNTs tended to form clusters which overlapped, which heavily favors the formation of three dimensional (3D) conductive pathways. Despite the non-uniform distribution of CNTs, the σ results from Figure 13 indicated that PP/CNT formed strong conductive network. Moreover, it appears that plaque microparts resulted in a greater number of smaller CNT clusters outside of large agglomerates and less FD orientation of nanotubes [157]. This is consistent with the greater disparity in σ

between step and plaque microparts along the FD in Figure 13. Additionally, Figures 14 and 15 showed the distribution of CNT agglomerates is not as uniform as PP/CB in plaque microparts. First, the average size of CNT agglomerates is significantly larger than that of CB-agglomerates. Second, there are fewer dispersed nanotubes outside of the major CNT clusters, whereas the PP/CB microparts exhibited a greater number of smaller and more dispersed clusters of CB particles.

3.1.3 Thermal Stability

The thermal decomposition behavior of both PP/CB and PP/CNT microparts was examined using a thermalgravimetric analyzer (TGA, TG 209F1 Iris, Netzsch). The mass loss (%) was charted as a function of temperature for all samples.

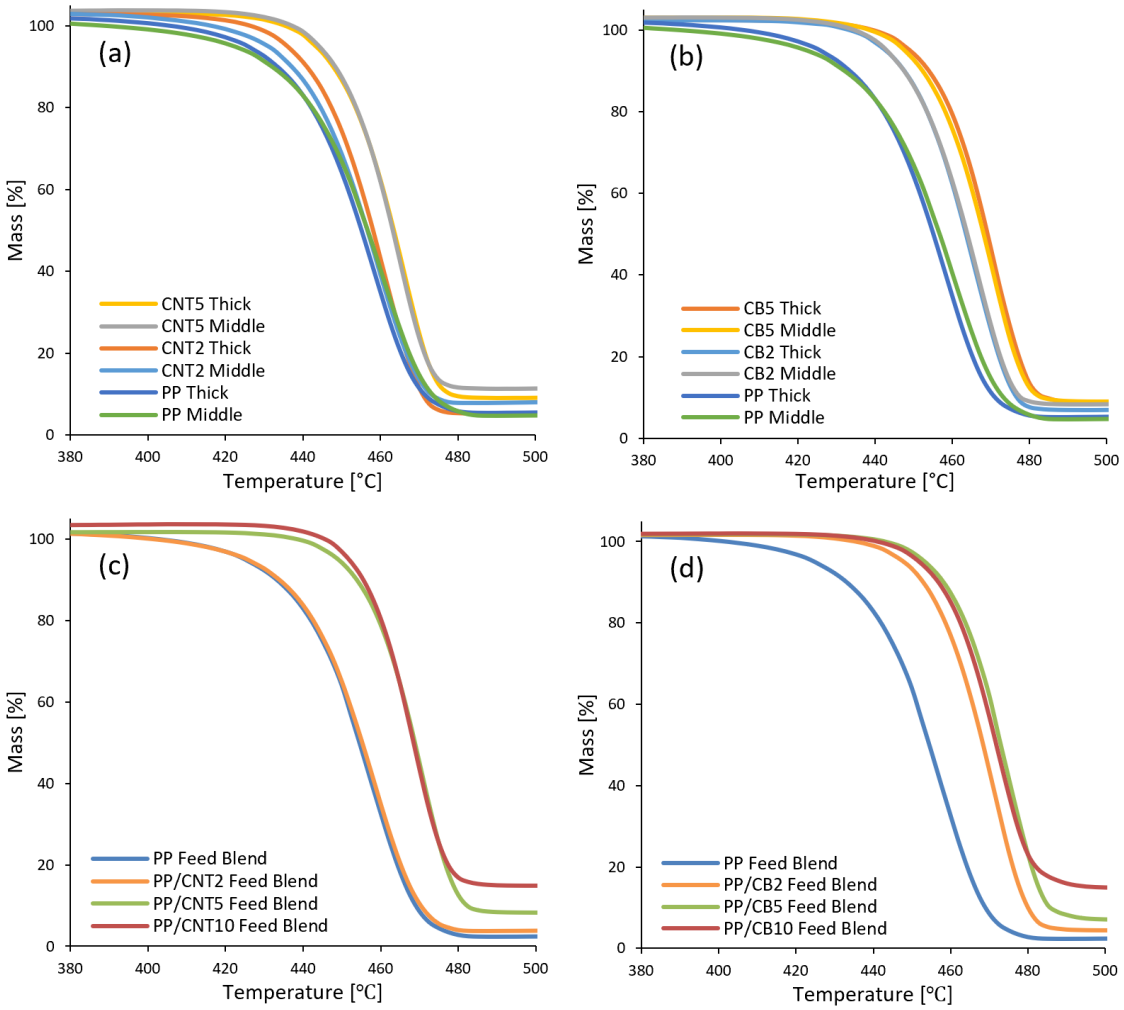

Figure 16: TGA graphs for (a) PP/CNT microparts (b) PP/CB plaque microparts (c) PP/CNT feed blends (d) PP/CB feed blends

The thermal stability of µIM microparts and corresponding feed blends were evaluated using TGA and graphically plotted Figure 16; the tabulated data are shown in Table 3. Results indicated that there is a significant improvement of thermal stability with the incorporation of CB particles in PP. In addition, the thermal stability increased with higher loadings of CB fillers in both PP/CB micropart and PP/CB blends. The TGA curve showed significant improvement in thermal stability from 0 to 2wt% CB loading, whereas only marginal improvement of thermal stability was detected for PP/CNT from 2 to 5wt% CNT loading. Both PP/CB and PP/CNT feed blends showed no further improvement from 5 to 10wt%. This is consistent with one study that reported highest

thermal stability at 5wt% CNT loading, but little further improvement with even more filler loading [14].

It can be inferred from Figure 16 that both PP/CNT and PP/CB systems showed three similarities. First, there was little further improvement of thermal stability when the filler content increased from 5 to 10 wt%. This suggested that after the formation of physical filler network (i.e., some filler loading threshold), there is little further benefit in adding more fillers. Second, the decomposition curves are nearly identical between thick and middle sections, showing minimal difference due to changes in micropart thickness.

Third, by comparing the difference between the TGA graphs of feed blends and molded microparts, the μIM process seems to have narrowed the difference between the 2 wt% and 5 wt% decomposition curves. This might be attributable to higher filler loading resulting in higher melt viscosity, which causes greater shearing effect with more preferential alignment of polymer chains along the flow direction. Greater flow-induced crystallization will, to a certain degree, favor greater enhancement of thermal stability, especially for PP/CNT composites. Additionally, filler rheological network could serve as a mass transfer barrier against volatile decomposed products. The polymer phase in close vicinity to fillers are restricted by the filler rheological network, thus increasing the energy required to decompose the polymer and altering the ability of degraded molecules to diffuse and evaporate [111].

Table 3: The 5wt% decomposition temperature ($T_{5\%}$), 30wt% decomposition temperature ($T_{30\%}$), maximum decomposition temperature (T_{max}), and char residue at 560°C (R_{560}) for PP/CB and PP/CNT microparts

	T_5 [°C]	**T_{30} [°C]**	**T_{max} [°C]**	**R_{560} [%]**
PP Thick	425.7	447.4	460.8	5.99
PP Middle	422.3	448.5	459.1	6.67
PP/CB2 Thick	442.7	457.5	467.0	7.48
PP/CB5 Thick	449.0	463.5	473.2	9.08
PP/CB2 Middle	443.0	457.6	467.1	9.18
PP/CB5 Middle	447.7	462.2	472.8	9.81
PP/CNT2 Thick	436.0	451.7	463.3	6.11
PP/CNT5 Thick	443.3	457.6	467.6	9.90
PP/CNT2 Middle	430.9	449.4	460.5	8.95
PP/CNT5 Middle	444.1	457.6	466.2	12.27

3.1.4 Melting and Crystallization Behavior

As discussed in Section 2.3.4, the melting and crystallization behavior of PP-based composites was analyzed using a differential scanning calorimeter (DSC, Q2000, TA Instruments). Figure 17 displays the DSC graphs and Table 4 shows the tabulated data for key thermal characteristics from DSC analysis.

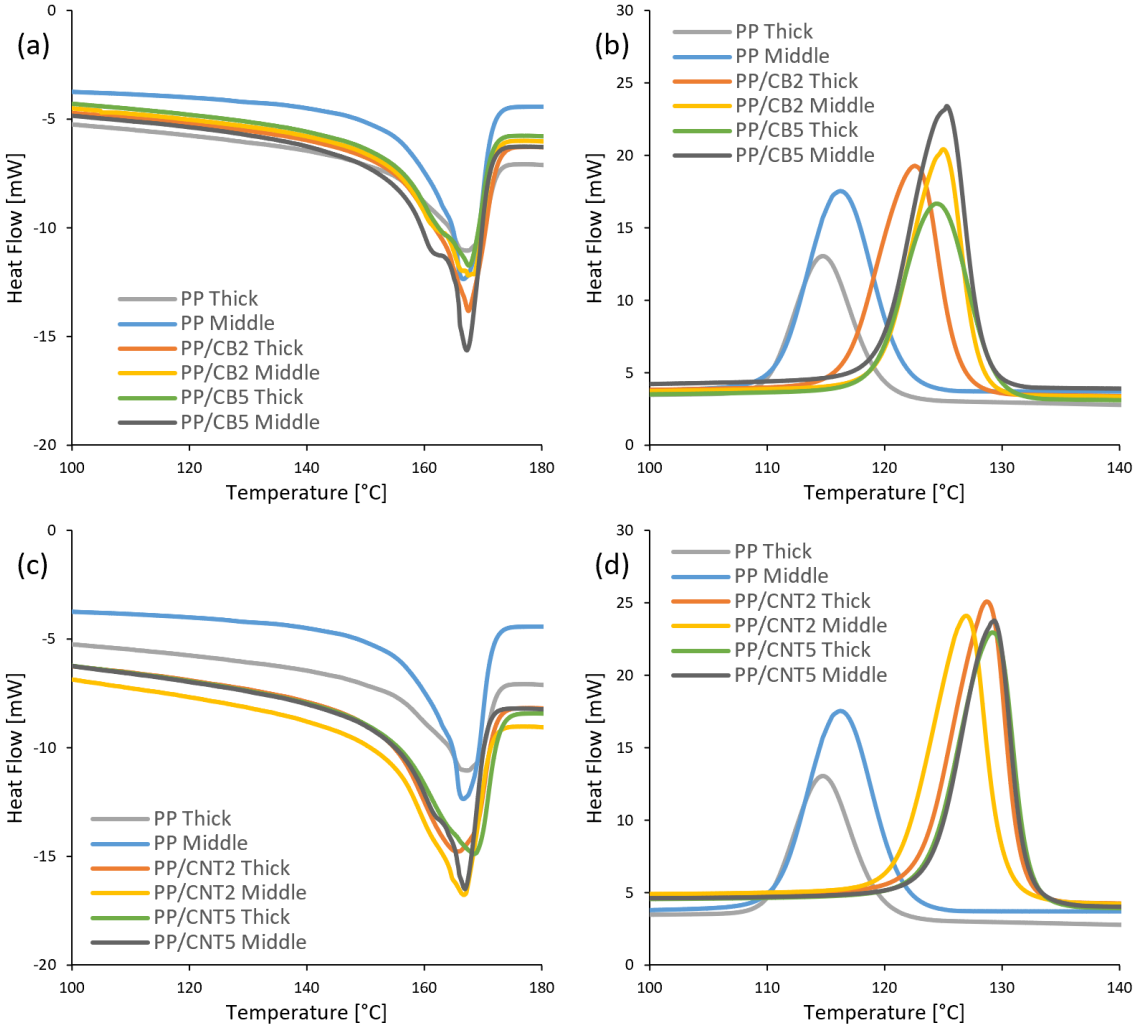

Figure 17: DSC scans of PP/CB microparts (a) first heating cycle (b) cooling cycle and PP/CNT micropart's (c) first heating cycle (d) cooling cycle

The 'shoulder' peaks as shown in Figure 17(a, c) can be attributed to the rapid melting, quick recrystallization, and then immediate remelting of imperfect α-crystals prior to the main melting peak for properly formed α-crystals [160]. Shoulder peaks were detected in PP/CNT microparts because CNT acts as strong nucleating agent, inducing PP to crystalize on the CNT surface [144]. Jiang et al. [16] reported larger shoulder peaks with increasing CNT concentration, which suggest that rapid crystallization can promote the formation of imperfect α-crystals, and consequently, shoulder peaks on DSC graphs. Moreover, the rapid cooling rate and high shear rate in μIM can also result in a greater number of imperfect α-crystals.

Moreover, all the major 'shoulders' appeared in the medium thickness microparts – CB2M, CB5M, and CNT5M microparts – rather than in thick microparts. This suggests that differing thickness might have promoted more imperfect α-crystals, possibly due to higher shear rate with thinner sections. It is unlikely to be due to accidental creation of β-crystal because that would result in a far more distinct second melting peak [161], which is not evident in the DSC melting graphs. The lack of a second melting peak at 140-150℃ is due to CNT acting as a strong α-nucleating agent, which can suppress β-nucleating effect and forced the material to exclusively yield α-crystals after reaching 2.5wt% CNT loading [140].

Table 4: Characteristic Data from DSC Scans for PP/CB and PP/CNT μIM microparts and their corresponding raw blends for first (heating) cycle, second (cooling) cycle, and third (heating) cycle.

Sample Designation	Cycle 1		Cycle 2	Cycle 3	
	T_m [℃]	χ_c [%]	T_c [℃]	T_m [℃]	χ_c [%]
PP-Pure-T	167.1	44.6	114.7	165.7	44.5
PP-Pure-M	166.7	43.3	116.2	164.4	38.0
PP-CB2-M	167.5	43.1	125.0	165.0	50.3
PP-CB2-T	167.5	40.2	122.5	165.6	42.1
PP-CB5-M	167.2	45.5	125.3	165.2	51.4
PP-CB5-T	167.6	37.9	124.4	166.9	43.8
PP-CB5 Feed Blend	167.3	40.4	121.2	166.9	44.0
PP-CNT2-T	165.6	44.0	128.7	165.4	50.7
PP-CNT2-M	166.7	45.1	127.0	165.2	39.4
PP-CNT5-T	168.4	41.2	129.2	168.4	47.1
PP-CNT5-M	166.9	42.1	129.3	165.6	47.3
PP-CNT5 Feed Blend	167.5	40.2	122.5	165.6	42.1

In general, the T_m is consistently higher for molded microparts in the 1st cycle than in the 3rd cycle, for both the molded microparts and feed blends. The T_c and χ_c increased significantly after the incorporation of 2wt% CNT. However, from 2 to 5 wt%, there was a much-diminished relative gain in both T_c and χ_c. This is consistent with one study noting that despite CNT acting as strong nucleating agent, further increase in CNT

loading beyond 0.2 wt% might not further improve the nucleation effect of CNT [141], which is consistent with the declining χ_c from CNT2 to CNT5 observed in the tabulated DSC thermal characteristic data. This might be due to saturation of CNT-induced nucleation sites, causing diminished return of higher CNT loading. Another possible reason is that after achieving rheological percolation, the 3D CNT filler network impedes the free movement of polymer chains, which might hamper their crystallization.

For PP/CB microparts, Chen et al. [162] reported that CB particles will also act as nuclei leading to the growth of α-crystals and merely 1wt% CB filler to PP matrix will significantly diminish the number of β-induced second melting peak. Zhou and co-workers reported that low CB filler loading corresponds to low nucleating effect of CB, but it can become significant after 2 wt% [163], which is consistent with the high χ_c in the table above.

Lastly, there was no correlation between electrical conductivity and χ_c, which is corroborated existing studies supports existing literature studies that

% Slower cooling rate is also favorable towards the formation of effective conductive pathways, which is shown in Figure 9, by promoting the growth of larger crystal sizes of a few microns, thus more effectively displacing CNT fillers from the crystallized region to the amorphous phase; larger crystal size is a more dominant factor over % crystallinity structure [144].

3.1.5 Summary

The electrical, thermal, and morphological properties of PP/CB and PP/CNT microparts was systematically studied via melt mixing and μIM. The results of plaque microparts in this study were compared to prior studies conducted with step microparts (after controlling for factors such as process conditions, materials, and experimental procedures) to determine whether the ‘step’ feature had any significant impact to the electrical, thermal, and morphological properties of the μIM microparts.

The DC electrical conductivity (σ) for plaque microparts were found to be consistently lower than its corresponding step microparts of the same thickness. The difference in σ

between the step and plaque microparts, for both the PP/CNT and PP/CB systems, were about one order of magnitude along the transverse direction and two orders of magnitude along the flow direction of polymer melt. This is supported by SEM images showing less FD orientation of CNT than prior studies with step microparts [157].

Additionally, DSC thermographs showed significant presence of ‘shoulder peaks’ in the medium microparts, but none for thick microparts or the feed blend. This suggests that the extremely high shear rate of the μIM process either caused or aggravated the number of imperfect α-crystals or increased the number of γ-crystals in the micromolded PP matrix. TGA results showed that the thermal stability of PP/CB microparts improved with less filler loading than PP/CNT microparts. Both PP/CB and PP/CNT samples failed to achieve further improvement after 5wt% filler loading.

3.2 Effect of PP/(CNT:CB) Hybrid Filler System

In this section, CNT and CB were both added to PP matrix to prepare PP/CNT/CB composites. The purpose of this study was to determine if there was any synergistic benefit in adding both CNT and CB fillers simultaneously to the PP matrix. The PP/(CNT:CB) hybrid filler system was examined at 3, 5 and 10wt% total filler loading using CNT100:CB0, CNT70:CB30, CNT50:CB50, CNT30:CB70, CNT0:CB100 ratios. For example, 10wt% total filler concentration at CNT70:CB30 ratio is equivalent to 7wt% CNT and 3wt% CB added to 90wt% PP. The filler materials were added to PP through melt compounding in a Brabender mixer, which was then used to produce feed material for plaque microparts through μIM.

3.2.1 Electrical conductivity

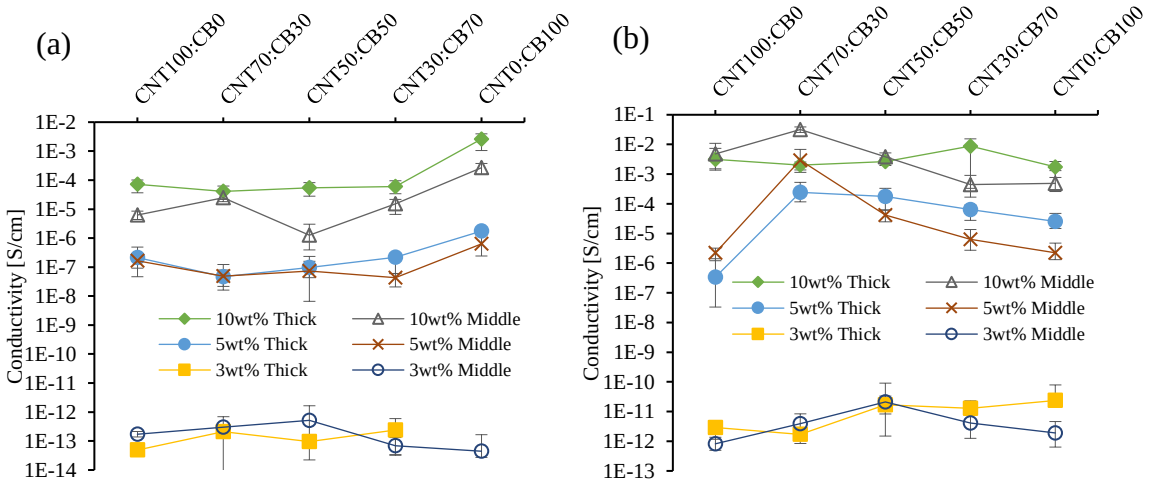

Figure 18: Electrical conductivity (σ) for PP/(CNT:CB) hybrid microparts at 3, 5, and 10 wt% filler loading along (a) TD and (b) FD, where TD denotes transverse direction and FD denotes flow direction.

The electrical conductivity (σ) was determined using a two-probe approach and reported in Figure 18. The values of σ were compared across samples of varying CNT:CB ratio at the same total filler loading fractions. Results suggested that there was no clear evidence of synergetic effect of using hybrid fillers along the TD. In single filler systems, PP/CNT microparts exhibited lower σ along TD when compared to PP/CB counterpart. In hybrid

filler systems, CNT70:CB30 filler ratio demonstrated the lowest σ compared to other CNT:CB ratios along the TD, with σ gradually increased with increasing fraction of CB and decreasing fraction of CNT. A comparison of σ between the T (0.83mm thickness) and M (0.50mm thickness) microparts suggested that the difference in part thickness of the microparts had minimal effect on the σ, often within 1 order of magnitude.

However, there is significant evidence of synergetic effect at the 5 wt% total filler concentration along the FD; the results are less clear at 10 wt%. At 5 wt% filler loading, the σ value along the FD is the highest at CNT70:CB30, then decreases with increasing loading ratio of CB and decreasing ratio of CNT. A synergistic effect for a PP/(CNT:CB) hybrid system at a similar ratio has been reported in the past using hot press, but not μIM. [72]

The lack of synergetic effect along the TD can be explained by the μIM's high shear conditions. The preferential alignment of CNT along the FD helps promote the synergetic effect along FD near the mold surface, assisting with electron hopping from CB particles aided by CNT bridges. However, given any fixed amount of filler, greater preferential alignment of CNT along the FD might be at the detriment of the TD. This is supported by the fact that the σ actually decreased along TD but increased along FD.

3.2.2 Morphology

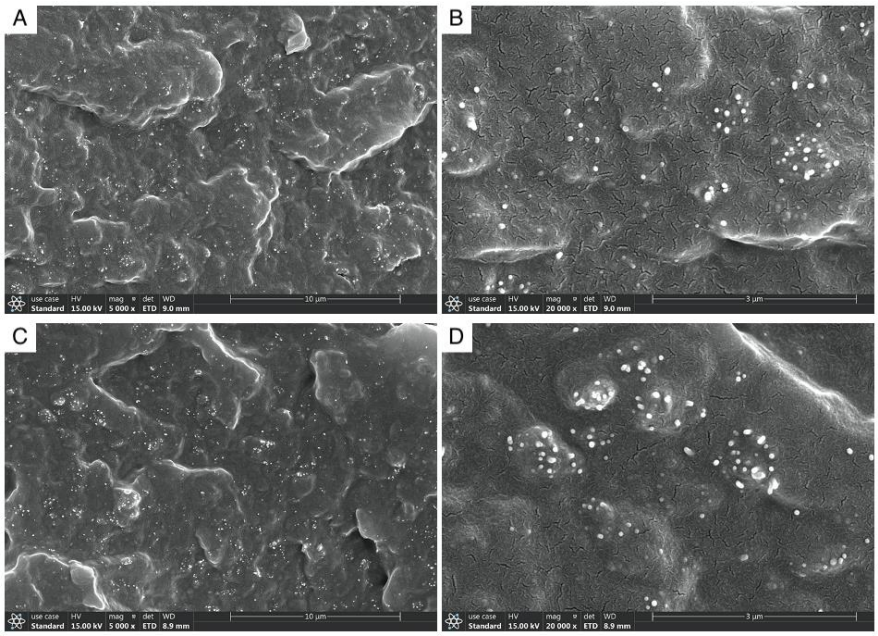

Figure 19: SEM images of PP/(CNT70:CB30)5T microparts. Herein: skin layers at (A) 5000x magnification (B) 20000x magnification; core layers at (C) 5000x magnification (D) 20000x magnification.

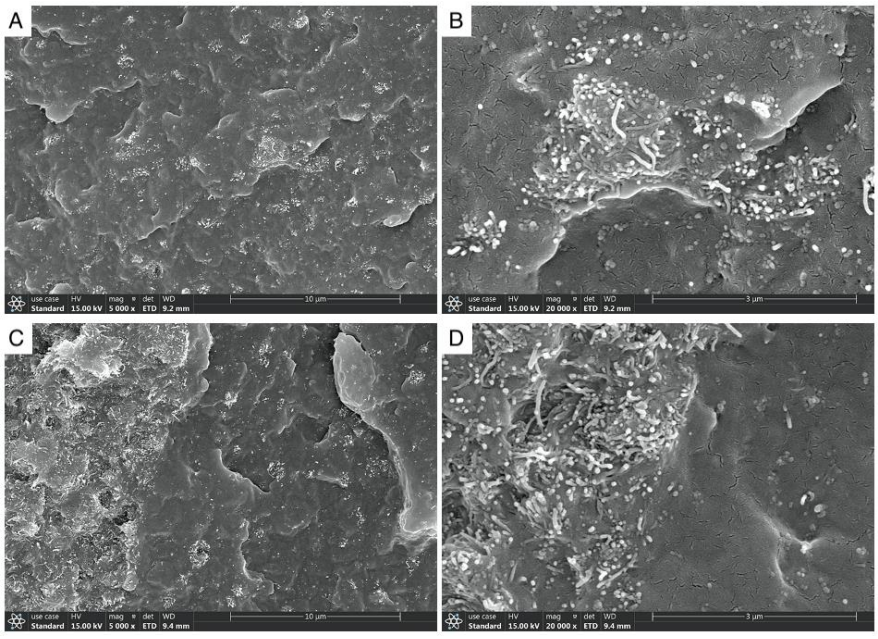

Figure 20: SEM images of PP/(CNT50:CB50)5T microparts. Herein: skin layers at (A) 5000x magnification (B) 20000x magnification; core layers at (C) 5000x magnification (D) 20000x magnification.

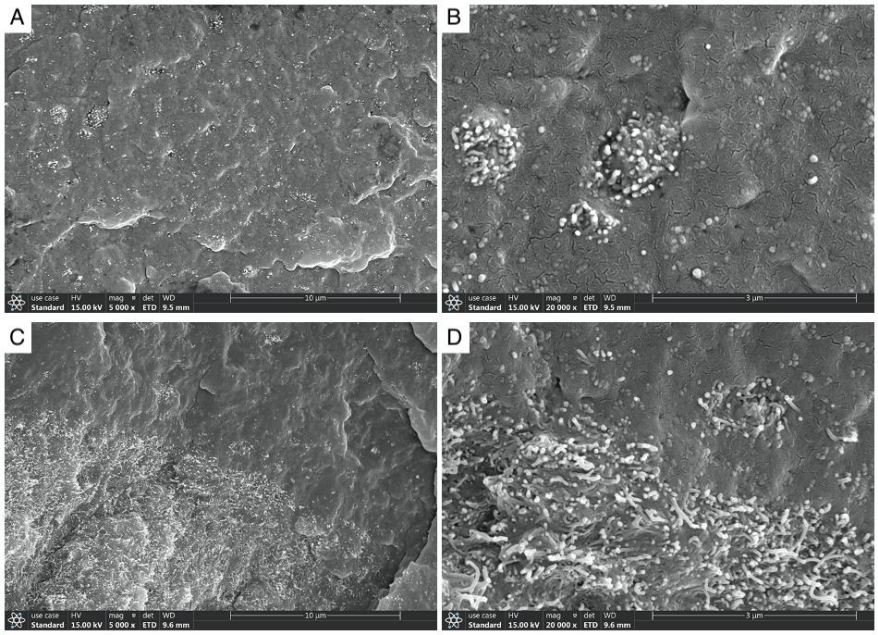

Figure 21: SEM images of PP/(CNT30:CB70)5T microparts. Herein: skin layers at (A) 5000x magnification (B) 20000x magnification; core layers at (C) 5000x magnification (D) 20000x magnification.

Wu and co-workers argued that in a hybrid system, it is possible to have segregated CB particle phases and CNT bridge phases [75]. Compared to CNT50:CB50 and CNT30:CB70 hybrid filler ratios, there is far less segregation of CB clusters and CNT clusters at CNT70:CB30. The size of each CNT cluster appears to be much smaller and contains far fewer nanotubes, and the clusters are more homogenously distributed. At CNT50:CB50 and CNT30:CB70, there are very severe, localized concentrations of CNT fillers, but the CB clusters are smaller and more evenly dispersed compared to CNT tube bundles; the characteristics of CB agglomerates are consistent with prior studies [19], [164].

Moreover, the extreme segregation that is shown in CNT50:CB50 and CNT30:CB70 is only noticeable in certain conditions. First, it is most noticeable in the core layer, but not the skin layer. Second, it is only present at 5wt% filler loading, but not 3wt% SEM graphs (included in the appendix). This suggests that the highly localized CNT filler distributions are more likely to occur at higher filler loading.

3.2.3 Melting and Crystallization Behavior

The melt and crystallization of PP/(CNT:CB) hybrid filler systems were determined using a differential scanning calorimeter (DSC, Q2000, TA Instruments). The data obtained from DSC scans are listed in the table below.

Table 5: Characteristic data obtained from DSC scans of PP/hybrid microparts and its corresponding blends. First cycle: heating cycle. Second cycle: cooling cycle. Third cycle: heating cycle.

Sample Name	1st Cycle		2nd Cycle	3rd Cycle	
	T_m [°C]	χ_c [%]	T_c [°C]	T_m [°C]	χ_c [%]
PP Middle	167.1	44.6	114.7	165.7	44.5
(CNT0:CB100)5M	167.2	45.5	125.3	165.2	51.4
(CNT30:CB70)5M	166.7	46.6	130.6	166.5	47.6
(CNT50:CB50)5M	165.1	39.6	131.3	166.4	41.8
(CNT70:CB30)5M	166.0	37.0	131.1	164.4	48.6
(CNT100:CB0)5M	166.9	42.1	129.3	165.6	47.3
PP Thick	166.7	43.3	116.2	164.4	38.0
(CNT0:CB100)5T	167.6	37.9	124.4	166.9	43.8
(CNT30:CB70)5T	166.6	36.8	128.6	166.1	42.8
(CNT50:CB50)5T	166.5	40.0	130.0	166.3	43.6
(CNT70:CB30)5T	166.7	38.0	130.3	166.3	38.0
(CNT100:CB0)5T	168.4	41.2	129.2	168.4	47.1
(CNT0:CB100) Feed Blend	167.3	40.4	121.2	167.3	44.0
(CNT30:CB70) Feed Blend	167.9	42.2	129.7	168.3	38.3
(CNT50:CB50) Feed Blend	166.7	38.2	130.8	166.7	46.3
(CNT70:CB30) Feed Blend	167.4	41.7	130.5	167.2	46.5
(CNT100:CB0) Feed Blend	167.5	40.2	122.5	165.6	42.1

Using PP/CNT (CNT100:CB0) and PP/CB (CNT0:CB100) as reference points, obtained from Section 3.1, two inferences can be made. First, the T_c value for all CNT:CB ratios in the hybrid filler system are consistently higher than both PP/CNT and PP/CB single filler systems, showing the CNT and CB fillers working synergistically to improve the crystallization temperature. The T_c increased significantly as CNT loading increased, and Dorigato et al. [165] hypothesized that using a CNT:CB hybrid fillers system might result in remarkable increase in T_c due to CB and CNT fillers working synergistically to

produce more effective percolative network. However, the melting temperature (T_m) for hybrid PP/(CNT:CB) microparts are marginally lower than PP/CB, PP/CNT, and pure PP microparts. The data table above shows that when compared to pure PP microparts, the hybrid fillers system have lower T_m whereas the single filler system marginally improved it.

Second, the crystallinity (χ_c) for the hybrid filler system is unlikely to be higher than both PP/CNT and PP/CB single filler system; this trend in χ_c also holds true for all microparts and feed blends. Additionally, there is no clear correlation between χ_c and changes in the CNT:CB ratio. Thus, it is unlikely that CNT's nucleating effect and χ_c were the dominant contributing factors that lead to the increase of σ along the FD at 5 wt% filler loading fraction. This is corroborated by findings that the CNT conductive network is more heavily influenced by crystal structure and size rather than χ_c [144]. Thus, any synergetic effect in σ is not predominately due to improvement in χ_c.

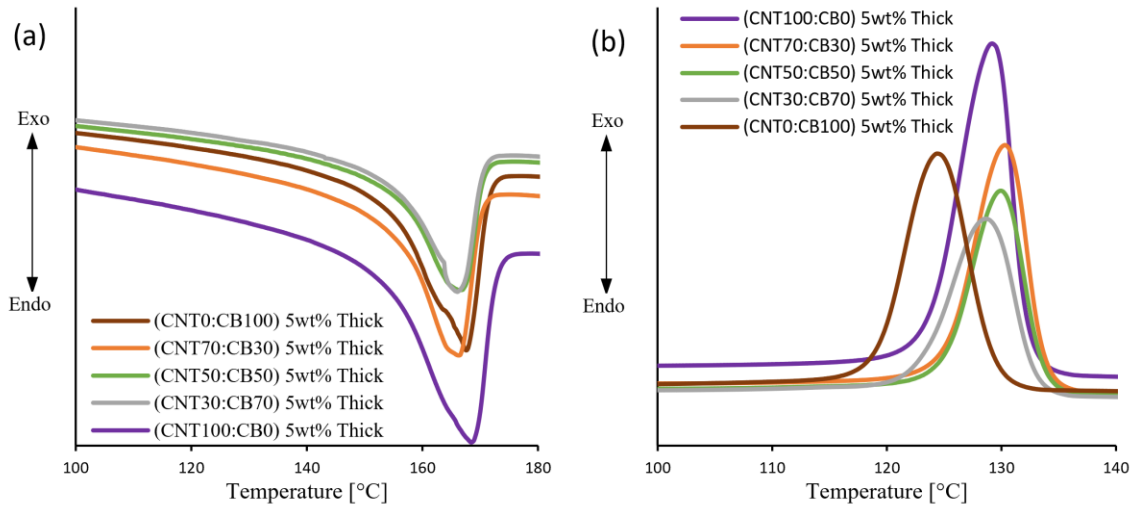

Figure 22: Comparison of DSC scans of PP/(CNT:CB) hybrid microparts with different CNT:CB ratio at 5 wt% total filler loading for (a) heating cycle (b) cooling cycle, taken from the middle of the microparts

The melting and crystallization behavior of PP/(CNT:CB) microparts are shown in Figure 22(a) and (b), respectively. Figure 22(a) showed that the addition of (CNT:CB) hybrid fillers had minimal effect on the general melting behavior of PP. However, the

crystallization process of PP was greatly accelerated with the incorporation of carbon fillers, as shown in Figure 22(b), which confirmed that heterogenous nucleation occurred in the composite systems. Moreover, CNT and CB fillers also worked synergistically, with higher CNT loading correlated with more accelerated crystallization process.

Overall, DSC scans showed no clear correlation to suggest any increase in χ_c was due to the use of CNT:CB hybrid filler system. T_c increased more with the hybrid filler system than PP/CB and PP/CNT single filler systems – higher CNT filler loading resulted in even greater improvement in T_c. However, it is unclear why the T_m for PP/(CNT:CB) hybrid filler system is consistently lower than PP/CB and PP/CNT single filler system.

3.2.4 Thermal Stability

The thermal decomposition behavior for PP/(CNT:CB) hybrid filler system was also examined using a thermalgravimetric analyzer (TGA, TG 209F1 Iris, Netzsch). Weight loss (%) was charted as a function of temperature for all samples.

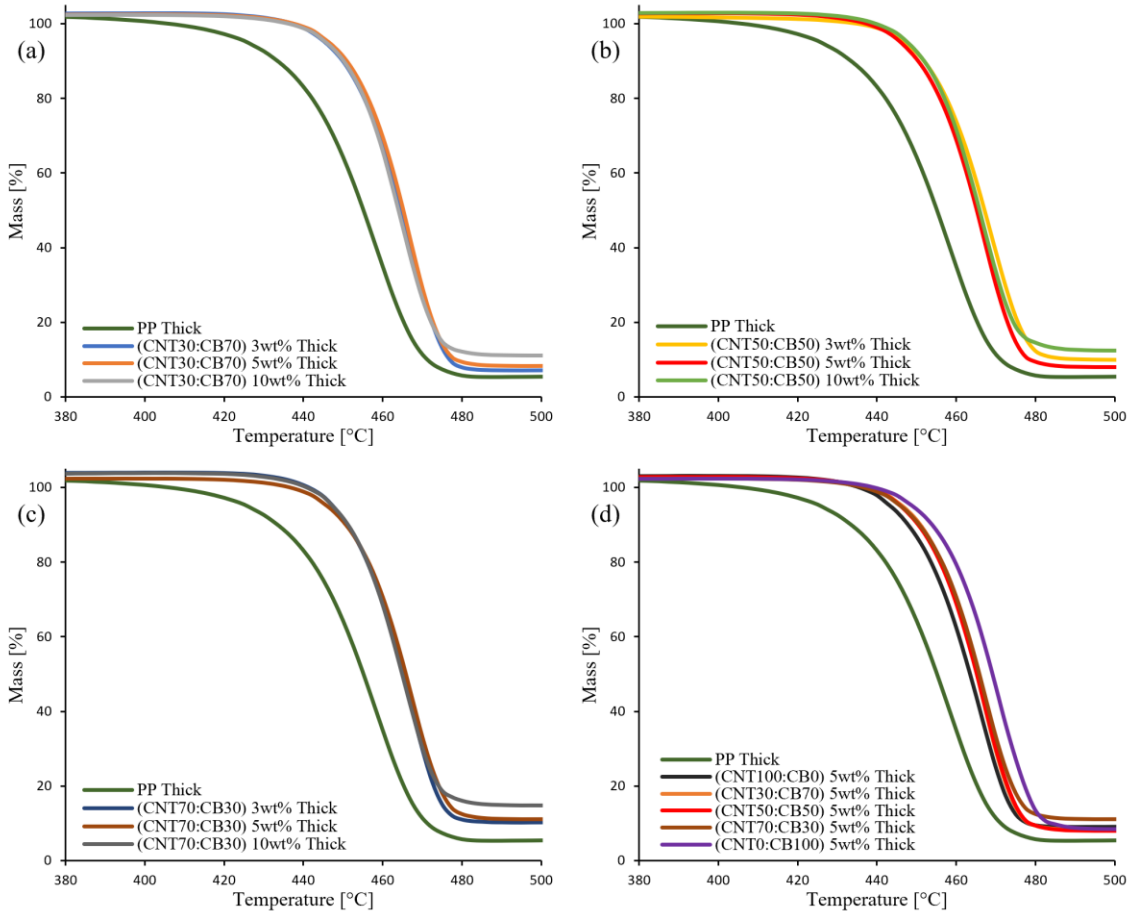

Figure 23: The TGA curves of (a) CNT30:CB70 microparts, (b) CNT50:CB50 microparts, (c) CNT70:CB30 microparts; (d) TGA curves for various CNT:CB ratios at 5 wt% total filler loading fraction.

At each filler ratio, e.g., CNT70:CB30, the TGA curves remained nearly identical and almost overlapping, regardless of total filler weight. For example, Figure 23(a) showed the TGA curves of 3, 5, and 10wt% at CNT70:CB30 ratio nearly overlaps. This shows that peak thermal stability was achieved at 3wt%. Figure 23(d) shows that at 5wt% total filler loading, varying CNT:CB ratio failed to result in significant changes to the TGA decomposition curves, but there is some small positive shift in TGA curve that corresponds to decrease in CNT and increase in CB loading. This is further supported by Table 6 below, which suggests that the thermal decomposition behavior is merely

correlated to the absolute CNT and CB filler content without obvious signs of synergistic effect.

Table 6: Comparison of the 5wt% decomposition temperature ($T_{5\%}$), 30wt% decomposition temperature ($T_{30\%}$), and maximum decomposition temperature (T_{max}) for µIM microparts at 5wt%

Sample Name	**$T_{5\%}$ [°C]**	**$T_{30\%}$ [°C]**	**T_{max} [°C]**
PP Middle	422.3	448.5	459.1
(CNT0:CB100) 5wt% Middle	447.7	462.2	472.8
(CNT30:CB70) 5wt% Middle	446.0	460.2	468.7
(CNT50:CB50) 5wt% Middle	448.5	461.7	470.0
(CNT70:CB30) 5wt% Middle	442.6	458.0	466.6
(CNT100:CB0) 5wt% Middle	444.1	457.6	466.2
PP Thick	425.7	447.4	460.8
(CNT0:CB100) 5wt% Thick	449.0	463.5	473.2
(CNT30:CB70) 5wt% Thick	446.4	459.5	465.4
(CNT50:CB50) 5wt% Thick	446.0	459.7	466.0
(CNT70:CB30) 5wt% Thick	446.0	460.2	465.4
(CNT100:CB0) 5wt% Thick	443.3	457.6	467.6

Table 7 shows that increased filler loading did not result in significant changes to T_5 and T_{30} values at all CNT:CB ratios. This is similar to findings in section 3.1 of this thesis, which showed that there is little further improvement in thermal stability by adding more fillers beyond a certain threshold for PP/CNT and PP/CB single filler microparts. However, with increased total filler wt%, there is some downward trend in T_{max} for hybrid samples. This might be attributable to worse filler distribution (i.e., densely packed, localized clusters of CNTs) at higher total loading, which might have caused less efficient rheological network.

Table 7: The 5wt% decomposition temperature ($T_{5\%}$), 30wt% decomposition temperature ($T_{30\%}$), and maximum decomposition temperature (T_{max}) for µIM hybrid filler microparts

Sample Name	**$T_{5\%}$ [°C]**	**$T_{30\%}$ [°C]**	**T_{max} [°C]**
Pure PP Middle	422.3	448.5	459.1
(CNT30:CB70) 3wt% Middle	444.8	459.1	469.9
(CNT30:CB70) 5wt% Middle	446.0	460.2	468.7
(CNT30:CB70) 10wt% Middle	444.7	459.3	466.9
(CNT50:CB50) 3wt% Middle	446.0	459.8	469.2
(CNT50:CB50) 5wt% Middle	448.5	461.7	470.0
(CNT50:CB50) 10wt% Middle	449.7	461.1	467.0
(CNT70:CB30) 3wt% Middle	447.9	461.0	468.3
(CNT70:CB30) 5wt% Middle	442.6	458.0	466.6
(CNT70:CB30) 10wt% Middle	447.2	460.1	466.3
PP Thick	425.7	447.4	460.8
(CNT30:CB70) 3wt% Thick	445.5	459.1	469.0
(CNT30:CB70) 5wt% Thick	446.4	459.5	465.4
(CNT30:CB70) 10wt% Thick	445.7	458.8	467.4
(CNT50:CB50) 3wt% Thick	447.0	461.4	469.4
(CNT50:CB50) 5wt% Thick	446.0	459.7	466.0
(CNT50:CB50) 10wt% Thick	447.7	460.5	466.9
(CNT70:CB30) 3wt% Thick	447.5	459.7	468.2
(CNT70:CB30) 5wt% Thick	446.0	460.2	465.4
(CNT70:CB30) 10wt% Thick	447.3	459.6	462.9

3.2.5 Rheological Properties

Melt rheology testing can be utilized to study the microstructure of the PP/carbon filler composite material. For the PP/(CNT:CB) hybrid filler system, this test was carried out with a rheometer (Bohlin Gemini 200, Malvern) using a parallel plate setup with the frequency sweep method from 0.1 to 100 Hz at 190°C.

Figure 24(a) shows the plot of storage modulus (G') vs loss modulus (G") with increasing frequency. At 5 and 10wt%, there is little difference in the G' vs G" slope between the two CNT:CB ratios. Pötschke and co-workers suggested that changes in the G' vs G" curve correspond to changes in the microstructure of the polymer composite [166]. One explanation might be that any synergistic effect in electrical conductivity in Figure 18 is mostly due to preferential alignment of the fillers along the FD during the µIM process, but this is not reflected in melt rheology.

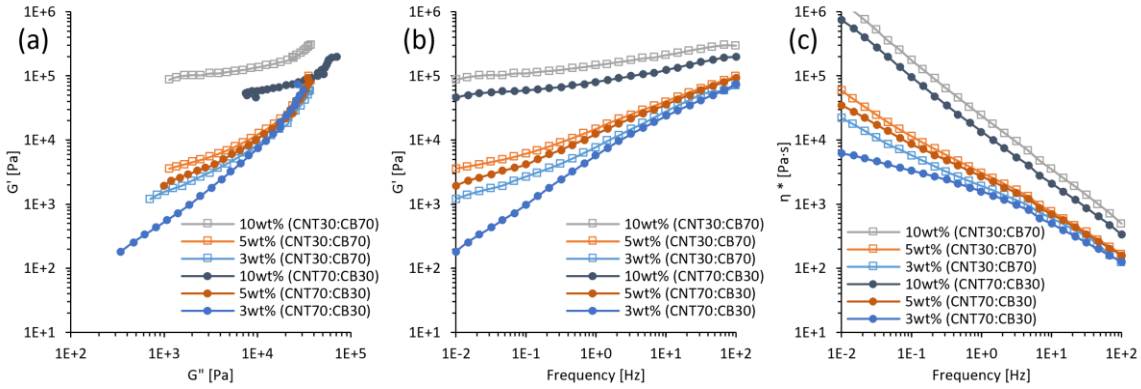

Figure 24: Melt rheology data for PP/(CNT:CB) composites at various CNT:CB ratios: (a) log-log plot of G' [Pa] versus G" (b) log-log plot of G' [Pa] versus frequency [Hz] (c) complex viscosity η * [Pa·s] versus frequency [Hz]

At 3wt% total filler loading, the CNT30:CB70 sample had less steep G' versu G" slope and higher η* than the CNT70:CB30 sample, which indicates the latter had significantly less developed microstructure [19]. More specifically, CNT30:CB70 experienced a much smaller increase in η * from 3wt% to 5wt% total filler loading, which suggests that it already reached its rheological percolation at 3wt%. However, the CNT70:CB30 sample still had a η* plateau at 3wt% total filler loading, which disappeared at 5wt%. The value of η* significantly increased from 3wt% to 5wt% at CNT70:CB30 ratio, which implies that the filler network was not fully developed at 3wt% [145].

Moreover, Zhou et al. previously reported PP/CB composites forming percolative network earlier than PP/CNT composites [19]. This is generally consistent with CNT70:CB30 blends having lower G' and η * than the CNT30:CB70 blends at 3, 5, and 10wt% total filler weight. Tuo and co-workers [167] argued that better dispersion of the carbon material provided greater viscosity of the composite material. Since the SEM micrographs in Figures 19-21 showed better dispersibility for CB than CNT fillers in a hybrid filler system, it makes sense for composites with higher CB ratio to result in higher viscosity. Furthermore, specific types of agglomeration can be desirable for enhancing the electrical conductivity, but more homogenous dispersion is preferred for rheological network [168]. At all CNT:CB ratios, there is significant agglomeration from CNT tube bundles, whereas the CB clusters are smaller and more evenly dispersed. This

might further explain why greater loading of CNT, with its high aspect ratio, might be preferred for electrical conductivity, but greater loading of well-dispersed CB is preferred for rheological networks.

3.2.6 Summary

The electrical, thermal, and morphological properties of PP loaded with a hybrid combination of CNT and CB fillers (at various CNT:CB ratios) were systematically studied via melt mixing and μIM. Direct current electrical conductivity was measured across the TD and along the FD of the polymer melt flow using a two-probe approach.

Results showed there was a significant synergistic effect in σ along the FD of the polymer melt at the expense of decreased σ across the TD. More specifically, at any total filler wt%, higher CNT and lower CB loading is associated with less filler phase separation and showed more synergistic effect in σ along the FD. SEM micrographs shows that smaller and more uniformly distributed CB clusters might be pushing CNTs into dense, localized clusters.

Additionally, DSC scans showed no clear correlation between T_m. χ_c, and various CNT:CB ratios. However, PP/(CNT:CB) hybrid fillers samples showed significantly higher T_c than both PP/CNT and PP/CB single filler system, with higher CNT loading correlated with greater synergistic improvement to T_c. TGA results showed that the thermal stability of microparts improved with increasing CB loading and decreasing CNT loading without any obvious signs of synergetic effect.

Melt rheology studies showed that at fixed total filler weight, greater CB loading results in higher complex viscosity and better developed rheological percolative network, which is consistent with a prior study that showed PP/CB composites can form percolative network earlier than PP/CNT composites [19]. This might also be correlated to SEM images showing that CB agglomerates are, on average, smaller in size and more uniformly distributed than CNT agglomerates. Hence, uniform dispersion is more important in forming rheological network, but it might not be favorable to electrical conductivity.

Overall, it was found that CNT70:CB30 ratio exhibited the highest synergetic effect on σ, crystallization behavior, and better filler distribution, all of which are gradually worsened with lower CNT and higher CB loading.

3.3 Effect of GNP fillers

Previous studies showed that microinjection-molded PP/GNP microparts resulted in much lower σ compared to compression molding [19]. Since µIM is expected to remain one of the primary methods of manufacturing small plastic microparts, the purpose of this study was to determine the potential of two methods that might improve the electrical, thermal, and morphological properties of µIM microparts.

Method one was to utilize PP powder instead of PP pellet in the melt mixing of PP matrix and GNP fillers. This is because smaller polymer particle size should result in (i) greater surface area for polymer-filler interaction and (ii) less localized filler accumulation. Method two was to create deliberate concentration (i.e., agglomeration) of conductive fillers at the interface between the polymer matrix particles. This approach, often known as ‘precoating’ in literature sources, will result in dense, localized filler concentration on the surface of the PP powder prior to melt compounding.

3.3.1 Electrical Conductivity

The DC electrical conductivity (σ) for all microparts was determined using a two-probe approach. The values of σ were compared across samples prepared with three different compounding methods of preparing PP/GNP composites – melt blending of PP pellets, melt blending of PP powder, and precoating and melt blending of PP powder with GNP fillers – as shown in Figure 25.

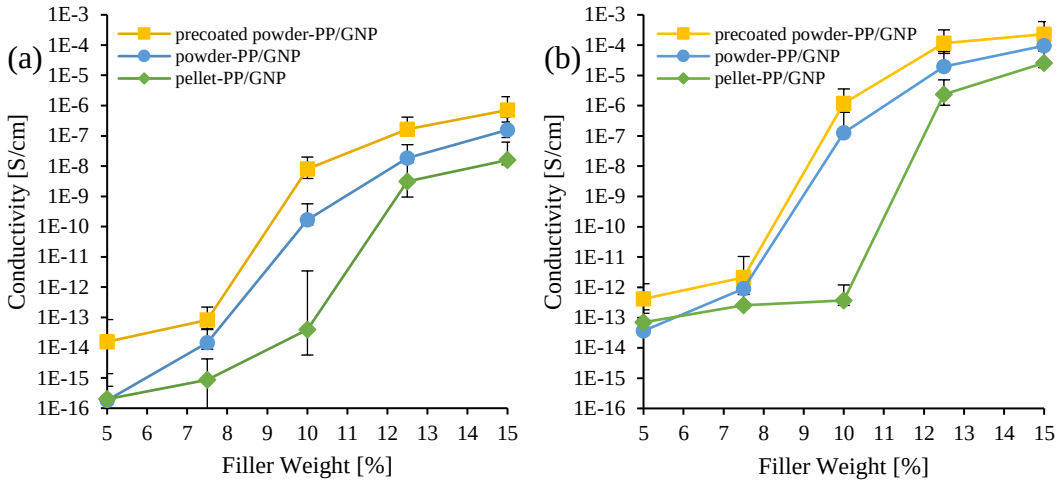

Figure 25: Electrical conductivity of PP/GNP for different preparation method along (a) Transverse Direction (b) Flow Direction

The microparts produced through simple melt blending of the powder-PP/GNP system achieved electrical percolation threshold (p_c) at 10wt% along both TD and FD, whereas the pellet-PP/GNP system only achieved p_c at 12.5wt%. After achieving percolation, the powder-PP/GNP system exhibited a consistent one order of magnitude improvement in σ over the pellet-PP/GNP system. It is possible that using a smaller particle size provided additional filler-matrix interface [97] to help with better dispersion. The smaller size difference between the polymer matrix and the filler likely reduced localized filler accumulation [118], [169].

Precoating of GNP and PP powder in the presence of isopropanol before melt compounding resulted in an additional one order-of-magnitude improvement in σ, but without further reduction in p_c. Kalaitzidou et al. argued melt compounding cannot provide enough shear to break down agglomerates and homogeneously disperse the GNP particles [82]. This is because melt blending only results in good macroscopic dispersion, but with poor microscopic dispersion and poor exfoliation of carbonaceous fillers such as graphene due to the high viscosity of many polymer matrices [13], [24]. On the other hand, ultrasonication of GNP fillers in solvent helped to break up GNP agglomerates [38], separate larger flakes and exfoliate individual graphene platelets apart by overcoming the binding energy among the graphene nanosheets [86], and achieve finer

nanoscopic dispersion of graphene at higher filler loading [87]. All of these can result in greater number of GNP particles and greater chance of forming a conductive network. Moreover, the powder coating method resulted better dispersion by providing a guaranteed minimum level of macroscopic dispersion before melt compounding [82], [91], [93], [94].

The σ for all microparts along the FD is consistently two to three orders of magnitude higher when compared to TD, which might be attributable to the high-shear conditions of the μIM process causing significant preferential alignment of GNP fillers along the flow direction [6], [16], [19]. This suggested that preferential alignment of GNP fillers along FD was much more significant than what was reported in prior studies involving PP/CNT microparts [154], [170].

The obtained σ results are slightly lower than prior studies by Kalaitzidou et al. with conventional injection-molded PP/GNP macroparts using very similar methodologies [82]. Since high-shear conditions of CIM can reduce the platelet size and aspect ratio of GNP flakes [17], the extreme shear rates of μIM process might further reduce platelet size. At the same filler loading, smaller GNP particle diameter results in a much greater number of particles available, thus increasing the likelihood of forming a conductive network [170], thus more likely to increase σ and reduce p_c. Furthermore, smaller particle size (i.e., smaller surface area) usually result in better dispersion and less agglomeration than larger diameter GNP flakes [64]. However, smaller particles can also result in lower σ after achieving percolation because a greater number of GNP particles will result in more interparticle ‘junctions’ and discontinuities, leading to higher contact resistance; larger particle size can result in a continuous conductive path with fewer contact points [91].

3.3.2 Morphological Properties

The morphology of PP/GNP microparts was examined using a SEM microscope in both the core layer and shear layer. All images were taken across the TD, as shown in Figure 12b. SEM micrographs for not-etched samples are shown in Figure 26 and etched samples are shown in Figure 27. The presence of GNP particles within PP are indicated in red.

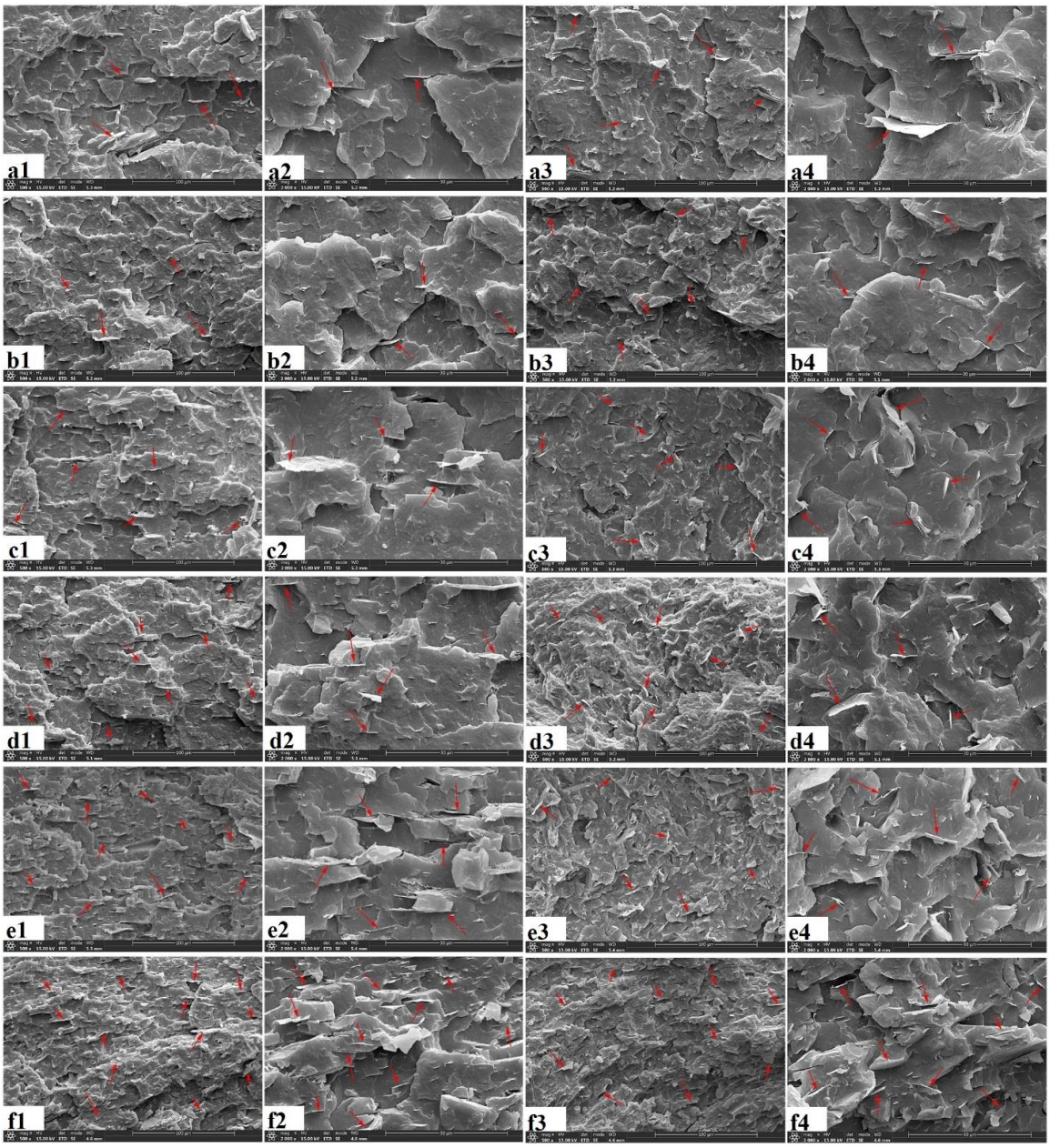

Figure 26: unetched SEM micrograph for (a) powder-PP/GNP3 (b) premixed powder-PP/GNP3 (c) powder-PP/GNP5 (d) premixed powder-PP/GNP5 (e) powder-PP/GNP10 (f) premixed powder-PP/GNP10. Herein: skin layers at (1) 500x magnification (2) 2000x magnification; core layers at (3) 500x magnification (4) 2000x magnification.

Figures 26(c1, c2) shows that GNP particles in the powder-PP/GNP5 system are somewhat more randomly dispersed in the core layer, but Figures 26(c3, c4) shows very clear preferential alignment of fillers in the skin layer. This can be ascribed to the different shear

rate in different layers of the microparts [19]. The preferred alignment of GNP along the FD likely resulted in significant improvement in σ at the expense of TD, which is similar to results from previous work completed on µIM composites produced from PP and graphite [170]. More holistically, Figure 26 showed ultrasonic precoated samples, at all filler wt% loading, having more numerous flakes with seemingly smaller flake size, which implies much better dispersion and exfoliation of GNP flakes.

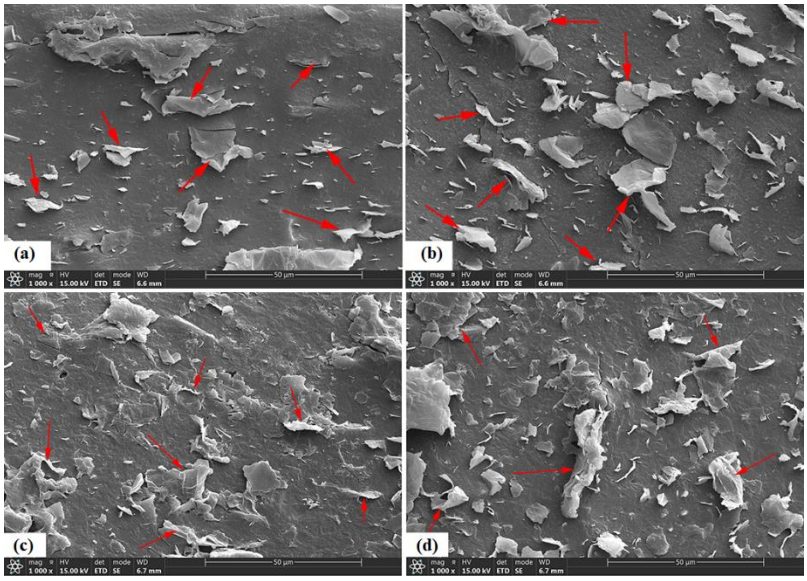

Figure 27: etched SEM micrograph for (a, b) pellet-PP/GNP5 (c, d) premixed powder-PP/GNP5: (a, c) skin layer; (b, d) core layer.

The pellet-PP/GNP5 system in Figure 27(a, b) exhibited more preferential alignment of GNP flakes and very large agglomerates, whereas premixed powder-PP/GNP5 in Figure 27(c, d) showed far less obvious signs of preferential alignment and smaller flake size. Thus, despite greater FD orientation, the pellet-PP/GNP system had much lower σ along the FD than the powder-PP/GNP system. This suggests that better dispersion and exfoliation of GNP flakes is a more dominant factor than the directional alignment of fillers. Moreover, despite utilizing solvent dispersion and ultrasonic exfoliation, pretreated powder-PP/GNP5 samples still showed significant agglomeration and restacking of GNP particles; the large GNP flake in the middle of Figure 27(d) is one prime example. This might be attributable to the high shear conditions of the µIM process, which can destroy excellent initial GNP dispersion [171]. While the GNP particles might be homogenously

distributed on a microscopic level, many smaller platelets can become attached to occasional large sheets [91], possibly due to a combination of significant shear-induced agglomeration [124] and the large surface area of GNP fillers [64].

3.3.3 Melting and Crystallization Behavior

As detailed in section 2.3.4, the melting and crystallization behavior of PP/GNP feed blends and the corresponding microparts were analyzed using a differential scanning calorimeter (DSC, Q200 and Q2000, TA Instruments). The first cycle (melting) reflects the thermomechanical history of the microparts due to melt compounding and the μIM process. The second cycle (crystallization) was used to analyze the crystallization behavior. The third cycle (melting) reflected the material properties without much influence of previous thermomechanical history, such as the effect of the μIM process. Figure 28 displays the DSC graphs and Table 8 shows the numerical data for key thermal characteristics from DSC analysis.

Table 8: The melting temperature (T_m), crystallization temperature (T_c), and crystallinity (χ_c) from DSC Scans for PP/GNP µIM microparts and its corresponding feed blends.

Sample Name	Cycle 1		Cycle 2	Cycle 3	
	T_m [°C]	χ_c [%]	T_c [°C]	T_m [°C]	χ_c [%]
Powder PP Micropart	165.2	43.8	111.3	161.2	48.5
Pellet PP Micropart	167.1	44.6	114.7	165.7	44.5
Pellet-PP/GNP5 Micropart	166.0	49.1	128.4	166.3	57.4
Pellet-PP/GNP10 Micropart	166.0	47.3	130.6	166.7	54.5
Pellet-PP/GNP15 Micropart	166.0	53.1	128.5	165.5	59.8
Powder-PP/GNP5 Micropart	164.1	44.7	124.8	162.2	49.0
Powder-PP/GNP10 Micropart	163.4	45.5	127.1	162.3	50.8
Powder-PP/GNP15 Micropart	161.9	45.2	129.0	162.7	50.1
Premixed powder-PP/GNP5 Micropart	163.6	46.3	123.8	162.2	52.2
Premixed powder-PP/GNP10 Micropart	163.2	45.8	127.6	161.7	51.9
Premixed powder-PP/GNP15 Micropart	163.4	46.9	129.2	162.6	51.6
Pellet-PP/GNP5 Feed Blend	166.4	53.2	127.8	165.5	53.6
Pellet-PP/GNP10 Feed Blend	167.0	57.3	130.3	166.2	55.0
Pellet-PP/GNP15 Feed Blend	167.0	51.6	131.5	167.0	51.7
Powder-PP/GNP5 Feed Blend	165.5	48.1	123.3	163.3	47.8
Powder-PP/GNP10 Feed Blend	166.5	46.7	125.4	164.4	47.6
Powder-PP/GNP15 Feed Blend	165.7	46.2	127.1	165.0	44.9
Premixed powder-PP/GNP5 Feed Blend	166.2	48.0	124.1	163.6	49.5
Premixed powder-PP/GNP10 Feed Blend	167.3	44.9	126.4	165.9	47.2
Premixed powder-PP/GNP15 Feed Blend	167.4	44.7	127.6	167.0	45.0

The χ_c for feed blends only marginally improved from the 1st cycle to the 3rd cycle, which suggests that prior thermomechanical history, especially the preparation method for the feed blends (without μIM), did not significantly affect the χ_c. On the other hand, the χ_c for all microparts significantly improved from the 1st cycle to the 3rd cycle of DSC scans, this implies that the μIM process is a very significant driver in reducing the χ_c.

Additionally, the micromolded samples had higher T_c and higher χ_c than its corresponding feed blends in the 2nd and 3rd cycle of DSC scans, respectively; higher T_c generally indicates greater heterogeneous nucleation effect of graphene-based fillers facilitating the crystallization of PP during cooling [28]. This might be attributable to the extremely high shearing effects in μIM [6], [9]. More specifically, GNP filler can be broken into smaller pieces due to processing methods and conditions [40], especially in melt extrusion [91], resulting in reduced aspect ratio and lower σ [91], [99]. Smaller particle size (i.e., smaller surface area) might also reduce GNP agglomeration and restacking [64], thus providing greater number of independent GNP particles for GNP-induced crystallization.

Overall, powder-PP/GNP feed blends showed more consistent downward trends in χ_c with increasing filler wt% loading compared to pellet-PP/GNP feed blends. This can be attributed to using PP powder resulted in less variability in material properties compared to using pellet form PP [169]. The pellet-PP/GNP microparts and feed blends exhibited higher χ_c than its powder-PP/GNP counterparts at all GNP filler wt% despite having much lower σ. This supports the theory that χ_c is a minor influence towards σ [144]. Since the planar structure of GNP is highly effective in restricting the movement of iPP's macromolecular chains and disturbing its regular coil conformation [172], thus, better dispersion of GNP fillers in powder-PP/GNP samples might have led to lower χ_c.

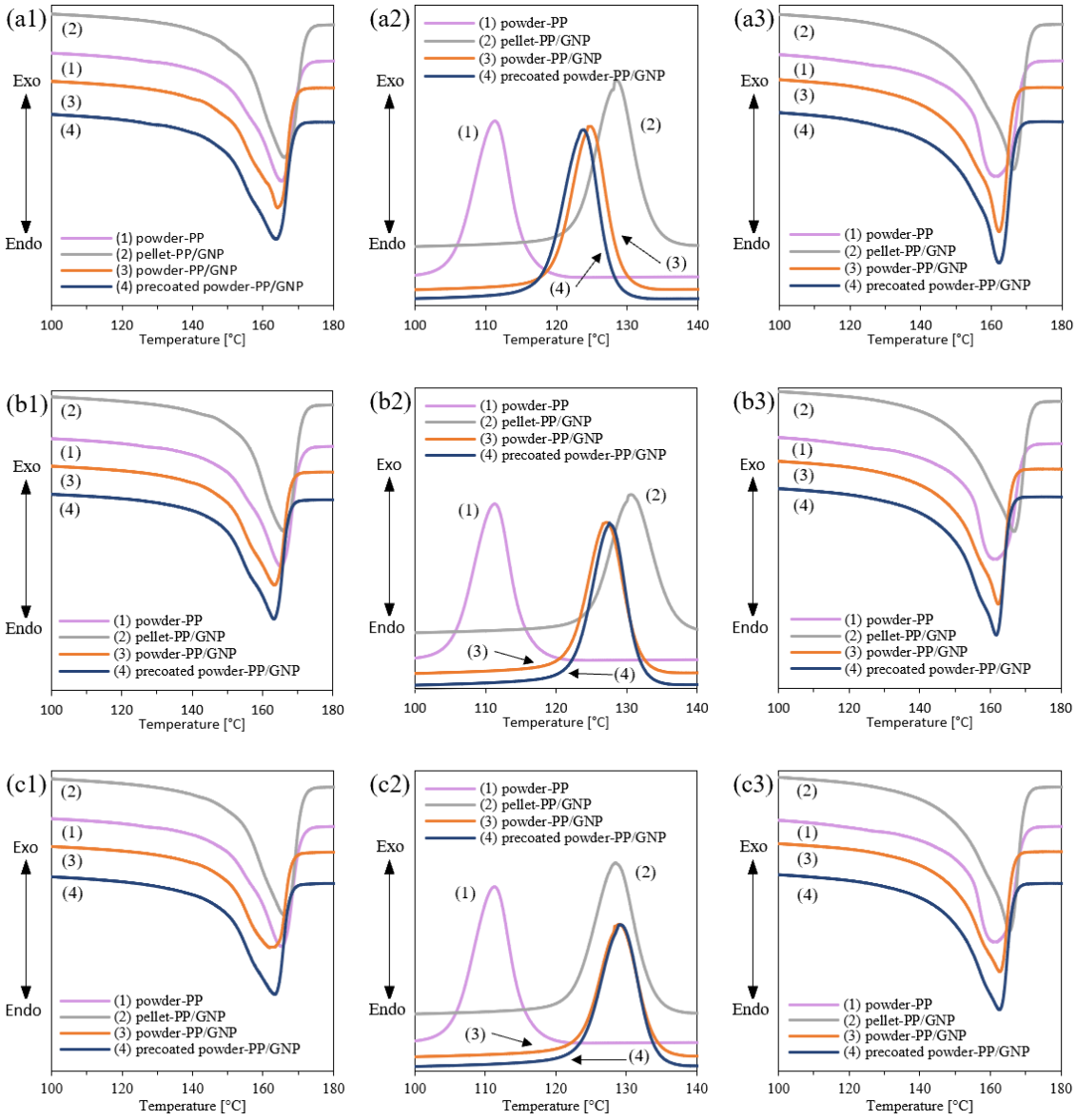

Figure 28: Comparison of DSC scans of PP/GNP microparts prepared through various methods at (a1-a3) 5wt% GNP loading; (b1-b3) 10wt% GNP loading; (c1-c3) 15wt% GNP loading. Herein, from left to right: 1-1st heating cycle; 2-cooling cycle; 3-2nd heating cycle.

The melting and crystallization behavior of PP/GNP microparts are displayed in Figure 28. The ‘shoulder’ peaks shown in Figure 28(a1, a3, b1, b3, c1, c3) can be attributed to the rapid melting, quick recrystallization, and then immediate remelting of imperfect α-crystals prior to the main melting peak for properly formed α-crystals [160], which shows

that GNP fillers can act as strong nucleating agents, inducing PP to crystalize on the GNP surface. However, the shoulder peaks were only witnessed in the powder-PP/GNP system but not in the pellet-PP/GNP system. This could be attributed to better dispersion of GNP fillers in the powder-PP/GNP system, which provided a greater number of crystallization sites available for rapid melting and recrystallization of imperfect α-crystals neighboring GNP fillers. Additionally, the lack of a distinct second melting peak at 140-150℃ suggests the lack of β-form iPP crystals [161], which is corroborated by findings that high GNP loading will induce changes to PP crystals conformation, resulting in the complete disappearance of the β-crystal form to become α-PP [142]. The lack of β-crystals is significant because those are twice as large as α-crystals, and larger crystals can have significant impact on toughness and conductivity [62]. Moreover, the very fast cooling rate of the μIM process also likely inhibited the formation of β-form PP crystals [173].

Since GNP is a nucleating agent and iPP crystals grow around the flakes, which means that a number of GNP particles will be encapsulated inside PP crystals and not able to participate in the formation of conductive network [62]. Similar phenomena was reported for PP/CNT [144] and PP/CB nanocomposites [24]. Thus, better dispersed and exfoliated fillers can result in a greater number of filler particles available to form continuous filler network. Similarly, ultrasonication during the premixing stage can also cause reduced aspect ratio of fillers [40], [99], which further increased the number of fillers available for conductive network and crystallization; this might be one reason why premixed powder-PP/GNP microparts had higher σ and χ_c compared to not-premixed powder-PP/GNP.

3.3.4 Summary

The purpose of this study was to determine the effectiveness of two methods that might be able to improve the electrical, thermal, and morphological properties of PP/GNP microparts. In the first method, PP powder was used instead of PP pellet in the melt blending of PP and GNP. In the second method, the ‘precoating’ method was used to cover the PP powder with GNP fillers prior to melt blending.

Results showed that using PP powder instead of PP pellet in the melt blending of PP/GNP (method 1) resulted in one order of magnitude higher electrical conductivity and reduced the electrical percolation from 12.5wt% to 10wt%. The ‘precoating’ of PP powder with GNP fillers (method 2) resulted in another one order of magnitude improvement in σ but failed to further reduce p_c. SEM micrographs shows precoated samples containing more numerous GNP flakes with smaller flake size, which can be attributed to the use of solvent and ultrasonication that helped to break down filler agglomerates and superior exfoliation of graphene sheets.

Moreover, DSC scans showed the thermomechanical history of the μIM process and the GNP filler particle size, dispersion, and exfoliation likely had an influence on the melting and crystallization behavior of the microparts.

4 Conclusions

This research examined the electrical and morphological properties of CB, CNT, and GNP filled polypropylene nanocomposites in microinjection molding. Rectangular-shaped plaque microparts with constant thickness were produced and characterized. The electrical conductivity of the microparts was characterized along the polymer melt flow direction (FD) and perpendicular to the flow direction (TD) using a two-probe approach. Electrical conductivity measurements were analyzed and correlated with the development of microstructures inside the microparts with the following conclusions.

The geometry of the micropart influenced the filler distribution and the electrical properties of the microparts. It was found that a plaque micropart of constant thickness resulted in lower volumetric electrical conductivity than previous studies that used step microparts with three different thicknesses in a single sample. The distribution of CB and CNT fillers in plaque microparts were also affected. For example, there appeared to be less FD alignment of CNT in plaque microparts than step microparts, along with less obvious signs of filler depletion in the skin layer.

The crystallization process of carbon-filled PP was significantly affected by filler distribution. For example, PP filled with CNT and CB fillers resulted in higher crystallization temperature than both PP/CNT and PP/CB single filler systems, with greater CNT loading correlated with greater synergistic improvement; this was not previously reported in literature sources for µIM processes. Additionally, the thermomechanical history of the µIM process and the GNP filler particle size, dispersion, and exfoliation likely had an influence on the melting and crystallization behavior of GNP-filled PP microparts.

Lastly, the compounding method can significantly influence the dispersion of GNP fillers. For example, ‘precoating’ the GNP fillers on the surface of PP powder through solvent blending and ultrasonication resulted in smaller GNP particle size, more randomized filler orientation, and more numerous GNP flakes. As far as the author is aware, the effectiveness of the ‘precoating’ method in µIM was studied and reported for the first time.

5 Recommendations for future research

This research examined the electrical and morphological properties of CB, CNT, and GNP filled polypropylene nanocomposites

First, interfacial interaction between fillers and polymer matrices is an essential component towards improving the dispersion of carbon fillers. Surface modification of carbon fillers and adding compatibilizers are two promising routes to further improve the dispersion of CB, CNT, and GNP fillers in micromolded composites. These aspects have been studied in conventional injection molding, but not yet studied in microinjection molding.

Second, more thorough studies on the dispersion of carbon fillers inside polymer matrices can be completed. For example, 3D micro-CT images can help to better visualize the distribution of carbon fillers. Similarly, Raman Spectroscopy can be used to provide precise, quantitative evidence om the exfoliation of GNP sheets.

References

[1] C. Yang, X. H. Yin, and G. M. Cheng, “Microinjection molding of microsystem components: New aspects in improving performance,” *J. Micromechanics Microengineering*, vol. 23, no. 9, 2013.

[2] F. Chiou, “Microinjection Molding,” in *Encyclopedia of Nanotechnology*, B. Bhushan, Ed. Dordrecht: Springer Netherlands, 2014, pp. 1–10.

[3] Y. C. Su, J. Shah, and L. Lin, “Implementation and analysis of polymeric microstructure replication by micro injection molding,” *J. Micromechanics Microengineering*, 2004.

[4] U. M. Attia, S. Marson, and J. R. Alcock, “Micro-injection moulding of polymer microfluidic devices,” *Microfluidics and Nanofluidics*, vol. 7, no. 1. pp. 1–28, 2009.

[5] G. Andrieux, J.-C. Eloy, and E. Mounier, “Technologies and market trends for polymer MEMS in microfluidics and lab-on-chip,” in *Microfluidics, BioMEMS, and Medical Microsystems III*, 2005.

[6] S. Abbasi, P. J. Carreau, and A. Derdouri, “Flow induced orientation of multiwalled carbon nanotubes in polycarbonate nanocomposites: Rheology, conductivity and mechanical properties,” *Polymer (Guildf).*, 2010.

[7] L. Yu, C. G. Koh, L. James Lee, K. W. Koelling, and M. J. Madou, “Experimental investigation and numerical simulation of injection molding with micro-features,” *Polym. Eng. Sci.*, 2002.

[8] Q. M. P. Nguyen, X. Chen, Y. C. Lam, and C. Y. Yue, “Effects of polymer melt compressibility on mold filling in micro-injection molding,” *J. Micromechanics Microengineering*, 2011.

[9] B. R. Whiteside, M. T. Martyn, and P. D. Coates, “In-process monitoring of

micromoulding - Assessment of process variation," in *International Polymer Processing*, 2005.

[10] G. Mittal, V. Dhand, K. Y. Rhee, S. J. Park, and W. R. Lee, "A review on carbon nanotubes and graphene as fillers in reinforced polymer nanocomposites," *Journal of Industrial and Engineering Chemistry*. 2015.

[11] H. Kim, A. A. Abdala, and C. W. MacOsko, "Graphene/polymer nanocomposites," *Macromolecules*. 2010.

[12] J. Sanes, C. Sánchez, R. Pamies, M. D. Avilés, and M. D. Bermúdez, "Extrusion of polymer nanocomposites with graphene and graphene derivative nanofillers: An overview of recent developments," *Materials*. 2020.

[13] M. Moniruzzaman and K. I. Winey, "Polymer nanocomposites containing carbon nanotubes," *Macromolecules*. 2006.

[14] G. Satish, V. V. S. Prasad, and K. Ramji, "Manufacturing and characterization of CNT based polymer composites," *Math. Model. Eng.*, 2017.

[15] D. Wanasinghe, F. Aslani, G. Ma, and D. Habibi, "Review of polymer composites with diverse nanofillers for electromagnetic interference shielding," *Nanomaterials*. 2020.

[16] Z. Jiang, Y. Chen, and Z. Liu, "The morphology, crystallization and conductive performance of a polyoxymethylene/carbon nanotube nanocomposite prepared under microinjection molding conditions," *J. Polym. Res.*, 2014.

[17] H. M. Park, K. Kalaitzidou, H. Fukushima, and L. T. Drzal, "Exfoliated graphite nanoplatelet (xGnP)/polypropylene nanocomposites," in *SPE Automotive and Composites Divisions - 7th Annual Automotive Composites Conference and Exhibition, ACCE 2007 - Driving Performance and Productivity*, 2007.

[18] S. Zhou, A. N. Hrymak, and M. R. Kamal, "Electrical, morphological and thermal properties of microinjection molded polyamide 6/multi-walled carbon nanotubes

nanocomposites," *Compos. Part A Appl. Sci. Manuf.*, 2017.

[19] S. Zhou, A. Hrymak, and M. Kamal, "Electrical and morphological properties of microinjection molded polypropylene/carbon nanocomposites," *J. Appl. Polym. Sci.*, vol. 134, no. 43, p. 45462, Nov. 2017.

[20] C. Phillips, A. Al-Ahmadi, S. J. Potts, T. Claypole, and D. Deganello, "The effect of graphite and carbon black ratios on conductive ink performance," *J. Mater. Sci.*, 2017.

[21] A. Kausar, "Contemporary applications of carbon black-filled polymer composites: An overview of essential aspects," *Journal of Plastic Film and Sheeting*. 2018.

[22] I. Balberg, "A comprehensive picture of the electrical phenomena in carbon black-polymer composites," *Carbon N. Y.*, 2002.

[23] J. C. Huang, "Carbon black filled conducting polymers and polymer blends," *Advances in Polymer Technology*. 2002.

[24] J. Yu, L. Q. Zhang, M. Rogunova, J. Summers, A. Hiltner, and E. Baer, "Conductivity of polyolefins filled with high-structure carbon black," *J. Appl. Polym. Sci.*, 2005.

[25] P. J. F. Harris, "Carbon nanotube composites," *International Materials Reviews*. 2004.

[26] S. Iijima, "Helical microtubules of graphitic carbon," *Nature*, 1991.

[27] R. Khare and S. Bose, "Carbon Nanotube Based Composites- A Review," *J. Miner. Mater. Charact. Eng.*, 2005.

[28] S. Zhang *et al.*, "Carbon-Nanotube-Based Electrical Conductors: Fabrication, Optimization, and Applications," *Advanced Electronic Materials*. 2019.

[29] M. Endo, M. S. Strano, and P. M. Ajayan, "Potential applications of carbon

nanotubes," in *Topics in Applied Physics*, 2008.

[30] Q. Zhang, J. Q. Huang, W. Z. Qian, Y. Y. Zhang, and F. Wei, "The road for nanomaterials industry: A review of carbon nanotube production, post-treatment, and bulk applications for composites and energy storage," *Small*. 2013.

[31] N. Anzar, R. Hasan, M. Tyagi, N. Yadav, and J. Narang, "Carbon nanotube - A review on Synthesis, Properties and plethora of applications in the field of biomedical science," *Sensors Int.*, 2020.

[32] T. R. Frmyr, F. K. Hansen, and T. Olsen, "The optimum dispersion of carbon nanotubes for epoxy nanocomposites: Evolution of the particle size distribution by ultrasonic treatment," *J. Nanotechnol.*, 2012.

[33] T. Skipa, D. Lellinger, W. Böhm, M. Saphiannikova, and I. Alig, "Influence of shear deformation on carbon nanotube networks in polycarbonate melts: Interplay between build-up and destruction of agglomerates," *Polymer (Guildf).*, 2010.

[34] J. Li, P. C. Ma, W. S. Chow, C. K. To, B. Z. Tang, and J. K. Kim, "Correlations between percolation threshold, dispersion state, and aspect ratio of carbon nanotubes," *Adv. Funct. Mater.*, 2007.

[35] J. Hilding, E. A. Grulke, Z. G. Zhang, and F. Lockwood, "Dispersion of carbon nanotubes in liquids," *J. Dispers. Sci. Technol.*, 2003.

[36] C. Li, E. T. Thostenson, and T. W. Chou, "Effect of nanotube waviness on the electrical conductivity of carbon nanotube-based composites," *Compos. Sci. Technol.*, 2008.

[37] F. H. Gojny *et al.*, "Evaluation and identification of electrical and thermal conduction mechanisms in carbon nanotube/epoxy composites," *Polymer (Guildf).*, 2006.

[38] H. Rennhofer and B. Zanghellini, "Dispersion state and damage of carbon nanotubes and carbon nanofibers by ultrasonic dispersion: A review,"

Nanomaterials. 2021.

[39] S. M. Sabet, H. Mahfuz, J. Hashemi, M. Nezakat, and J. A. Szpunar, “Effects of sonication energy on the dispersion of carbon nanotubes in a vinyl ester matrix and associated thermo-mechanical properties,” *J. Mater. Sci.*, 2015.

[40] Z. Baig, O. Mamat, M. Mustapha, A. Mumtaz, K. S. Munir, and M. Sarfraz, “Investigation of tip sonication effects on structural quality of graphene nanoplatelets (GNPs) for superior solvent dispersion,” *Ultrason. Sonochem.*, 2018.

[41] J. Li and J. K. Kim, “Percolation threshold of conducting polymer composites containing 3D randomly distributed graphite nanoplatelets,” *Compos. Sci. Technol.*, 2007.

[42] F. Giubileo, A. Di Bartolomeo, L. Iemmo, G. Luongo, and F. Urban, “Field emission from carbon nanostructures,” *Applied Sciences (Switzerland)*, vol. 8, no. 4. MDPI AG, 29-Mar-2018.

[43] R. Sengupta, M. Bhattacharya, S. Bandyopadhyay, and A. K. Bhowmick, “A review on the mechanical and electrical properties of graphite and modified graphite reinforced polymer composites,” *Progress in Polymer Science (Oxford)*, vol. 36, no. 5. pp. 638–670, May-2011.

[44] M. Ioniţă, G. M. Vlăsceanu, A. A. Watzlawek, S. I. Voicu, J. S. Burns, and H. Iovu, “Graphene and functionalized graphene: Extraordinary prospects for nanobiocomposite materials,” *Compos. Part B Eng.*, vol. 121, pp. 34–57, Jul. 2017.

[45] V. Dhinakaran, M. Lavanya, K. Vigneswari, M. Ravichandran, and M. D. Vijayakumar, “Review on exploration of graphene in diverse applications and its future horizon,” in *Materials Today: Proceedings*, 2020.

[46] J. H. Ahn and B. H. Hong, “Graphene for displays that bend,” *Nat. Nanotechnol.*, 2014.

[47] B. Aïssa, N. K. Memon, A. Ali, and M. K. Khraisheh, “Recent progress in the growth and applications of graphene as a smart material: A review,” *Frontiers in Materials*. 2015.

[48] C. Casiraghi *et al.*, “Rayleigh imaging of graphene and graphene layers,” *Nano Lett.*, 2007.

[49] A. K. Geim and K. S. Novoselov, “The rise of graphene,” *Nat. Mater.*, 2007.

[50] Y. Zhang, L. Zhang, and C. Zhou, “Review of chemical vapor deposition of graphene and related applications,” *Acc. Chem. Res.*, 2013.

[51] G. Kalita and M. Tanemura, “Fundamentals of Chemical Vapor Deposited Graphene and Emerging Applications,” in *Graphene Materials - Advanced Applications*, 2017.

[52] M. S. A. Bhuyan, M. N. Uddin, M. M. Islam, F. A. Bipasha, and S. S. Hossain, “Synthesis of graphene,” *Int. Nano Lett.*, 2016.

[53] C. Berger *et al.*, “Electronic confinement and coherence in patterned epitaxial graphene,” *Science (80-.).*, 2006.

[54] S. Park and R. S. Ruoff, “Chemical methods for the production of graphenes,” *Nat. Nanotechnol.*, vol. 4, no. 4, pp. 217–224, Mar. 2009.

[55] A. A. Balandin *et al.*, “Superior thermal conductivity of single-layer graphene,” *Nano Lett.*, vol. 8, no. 3, pp. 902–907, 2008.

[56] S. Ghosh *et al.*, “Dimensional crossover of thermal transport in few-layer graphene,” *Nat. Mater.*, vol. 9, no. 7, pp. 555–558, 2010.

[57] C. Vallés, A. M. Abdelkader, R. J. Young, and I. A. Kinloch, “Few layer graphene-polypropylene nanocomposites: The role of flake diameter,” *Faraday Discuss.*, 2014.

[58] S. Ye *et al.*, “Thickness-dependent strain effect on the deformation of the

graphene-encapsulated Au nanoparticles," *J. Nanomater.*, 2014.

[59] D. Li, M. B. Müller, S. Gilje, R. B. Kaner, and G. G. Wallace, "Processable aqueous dispersions of graphene nanosheets," *Nat. Nanotechnol.*, vol. 3, no. 2, pp. 101–105, 2008.

[60] Y. Si and E. T. Samulski, "Synthesis of water soluble graphene," *Nano Lett.*, vol. 8, no. 6, pp. 1679–1682, Jun. 2008.

[61] K. Singh, A. Ohlan, and S. K. Dhawan, "Polymer-Graphene Nanocomposites : Preparation , Characterization , Properties , and Applications," 2012.

[62] K. Kalaitzidou, H. Fukushima, P. Askeland, and L. T. Drzal, "The nucleating effect of exfoliated graphite nanoplatelets and their influence on the crystal structure and electrical conductivity of polypropylene nanocomposites," *J. Mater. Sci.*, 2008.

[63] Y. Wang and G. J. Weng, "Electrical Conductivity of Carbon Nanotube- and Graphene-Based Nanocomposites BT - Micromechanics and Nanomechanics of Composite Solids," in *Micromechanics and Nanomechanics of Composite Solids*, 2018.

[64] J. K. W. Sandler, J. E. Kirk, I. A. Kinloch, M. S. P. Shaffer, and A. H. Windle, "Ultra-low electrical percolation threshold in carbon-nanotube-epoxy composites," *Polymer (Guildf).*, 2003.

[65] S. H. Xie, Y. Y. Liu, and J. Y. Li, "Comparison of the effective conductivity between composites reinforced by graphene nanosheets and carbon nanotubes," *Appl. Phys. Lett.*, 2008.

[66] D. D. L. Chung, "A review of exfoliated graphite," *J. Mater. Sci.*, 2015.

[67] L. Yue, G. Pircheraghi, S. A. Monemian, and I. Manas-Zloczower, "Epoxy composites with carbon nanotubes and graphene nanoplatelets - Dispersion and synergy effects," *Carbon N. Y.*, 2014.

[68] M. Safdari and M. S. Al-Haik, “Synergistic electrical and thermal transport properties of hybrid polymeric nanocomposites based on carbon nanotubes and graphite nanoplatelets,” *Carbon N. Y.*, 2013.

[69] H. Fan, N. Zhao, H. Wang, J. Xu, and F. Pan, “3D conductive network-based free-standing PANI-RGO-MWNTs hybrid film for high-performance flexible supercapacitor,” *J. Mater. Chem. A*, 2014.

[70] S. Kumar *et al.*, “Dynamic synergy of graphitic nanoplatelets and multi-walled carbon nanotubes in polyetherimide nanocomposites,” *Nanotechnology*, 2010.

[71] E. Ivanov *et al.*, “PLA/Graphene/MWCNT composites with improved electrical and thermal properties suitable for FDM 3D printing applications,” *Appl. Sci.*, 2019.

[72] M. H. Al-Saleh, “Synergistic effect of CNT/CB hybrid mixture on the electrical properties of conductive composites,” *Mater. Res. Express*, 2019.

[73] J. Sumfleth, X. C. Adroher, and K. Schulte, “Synergistic effects in network formation and electrical properties of hybrid epoxy nanocomposites containing multi-wall carbon nanotubes and carbon black,” *J. Mater. Sci.*, 2009.

[74] P. C. Ma *et al.*, “Enhanced electrical conductivity of nanocomposites containing hybrid fillers of carbon nanotubes and carbon black,” *ACS Appl. Mater. Interfaces*, 2009.

[75] D. Wu *et al.*, “Polylactide composite foams containing carbon nanotubes and carbon black: Synergistic effect of filler on electrical conductivity,” *Carbon N. Y.*, 2015.

[76] H. Yang *et al.*, “Effect of carbon black on improving thermal stability, flame retardancy and electrical conductivity of polypropylene/carbon fiber composites,” *Compos. Sci. Technol.*, 2015.

[77] A. V. Rane, K. Kanny, V. K. Abitha, and S. Thomas, “Methods for Synthesis of

Nanoparticles and Fabrication of Nanocomposites," in *Synthesis of Inorganic Nanomaterials*, 2018.

[78] K. Ke *et al.*, "A comparison of melt and solution mixing on the dispersion of carbon nanotubes in a poly(vinylidene fluoride) matrix," *Compos. Part B Eng.*, 2012.

[79] E. Narimissa, R. K. Gupta, N. Kao, H. J. Choi, and S. N. Bhattacharya, "The comparison between the effects of solvent casting and melt intercalation mixing processes on different characteristics of polylactide-nanographite platelets composites," *Polym. Eng. Sci.*, vol. 55, no. 7, pp. 1560–1570, 2015.

[80] C. L. Huang, C. W. Lou, C. F. Liu, C. H. Huang, X. M. Song, and J. H. Lin, "Polypropylene/graphene and polypropylene/carbon fiber conductive composites: Mechanical, crystallization and electromagnetic properties," *Appl. Sci.*, vol. 5, no. 4, pp. 1196–1210, 2015.

[81] Q. Beuguel, A. Mija, B. Vergnes, and E. Peuvrel-Disdier, "Structural, thermal, rheological and mechanical properties of polypropylene/graphene nanoplatelets composites: Effect of particle size and melt mixing conditions," *Polym. Eng. Sci.*, vol. 58, no. 11, pp. 1937–1944, Nov. 2018.

[82] K. Kalaitzidou, H. Fukushima, and L. T. Drzal, "A new compounding method for exfoliated graphite-polypropylene nanocomposites with enhanced flexural properties and lower percolation threshold," *Compos. Sci. Technol.*, vol. 67, no. 10, pp. 2045–2051, Aug. 2007.

[83] J. A. Covas and M. C. Paiva, "Monitoring Dispersion and Re-agglomeration Phenomena During the Manufacture of Polymer Nanocomposites," in *Processing of Polymer Nanocomposites*, Carl Hanser Verlag GmbH & Co. KG, 2019, pp. 97–120.

[84] A. I. Isayev, R. Kumar, and T. M. Lewis, "Ultrasound assisted twin screw extrusion of polymer-nanocomposites containing carbon nanotubes," *Polymer*

(Guildf)., 2009.

[85] J. Zhong, A. I. Isayev, and X. Zhang, “Ultrasonic twin screw compounding of polypropylene with carbon nanotubes, graphene nanoplates and carbon black,” *Eur. Polym. J.*, 2016.

[86] W. Zhang, W. He, and X. Jing, “Preparation of a stable graphene dispersion with high concentration by ultrasound,” *J. Phys. Chem. B*, 2010.

[87] K. Muthoosamy and S. Manickam, “State of the art and recent advances in the ultrasound-assisted synthesis, exfoliation and functionalization of graphene derivatives,” *Ultrasonics Sonochemistry*. 2017.

[88] Y. Hernandez *et al.*, “High-yield production of graphene by liquid-phase exfoliation of graphite,” *Nat. Nanotechnol.*, 2008.

[89] B. Zhang and T. Chen, “Study of ultrasonic dispersion of graphene nanoplatelets,” *Materials (Basel).*, 2019.

[90] M. Lotya *et al.*, “Liquid phase production of graphene by exfoliation of graphite in surfactant/water solutions,” *J. Am. Chem. Soc.*, vol. 131, no. 10, pp. 3611–3620, Mar. 2009.

[91] H. Wu, B. Rook, and L. T. Drzal, “Dispersion optimization of exfoliated graphene nanoplatelet in polyetherimide nanocomposites: Extrusion, precoating, and solid state ball milling,” *Polym. Compos.*, 2013.

[92] D. W. Johnson, B. P. Dobson, and K. S. Coleman, “A manufacturing perspective on graphene dispersions,” *Current Opinion in Colloid and Interface Science*. 2015.

[93] X. Jiang and L. T. Drzal, “Reduction in percolation threshold of injection molded high-density polyethylene/exfoliated graphene nanoplatelets composites by solid state ball milling and solid state shear pulverization,” *J. Appl. Polym. Sci.*, vol. 124, no. 1, pp. 525–535, Apr. 2012.

[94] H. M. Park, K. Kalaitzidou, H. Fukushima, and L. T. Drzal, “Dispersion optimization of exfoliated graphite nanoplatelets in polypropylene: Extrusion vs precoating of PP powder,” in *International SAMPE Technical Conference*, 2008.

[95] Y. Li, J. Zhu, S. Wei, J. Ryu, L. Sun, and Z. Guo, “Poly(propylene)/graphene nanoplatelet nanocomposites: Melt rheological behavior and thermal, electrical, and electronic properties,” *Macromol. Chem. Phys.*, vol. 212, no. 18, pp. 1951–1959, 2011.

[96] D. Cassano, R. La Spina, J. Ponti, I. Bianchi, and D. Gilliland, “Inorganic Species-Doped Polypropylene Nanoparticles for Multifunctional Detection,” *ACS Appl. Nano Mater.*, 2021.

[97] K. A. Shiyanova *et al.*, “Segregated Network Polymer Composites with High Electrical Conductivity and Well Mechanical Properties based on PVC, P(VDF-TFE), UHMWPE, and rGO,” *ACS Omega*, 2020.

[98] M. G. Lee, S. Lee, J. Cho, and J. Y. Jho, “Improving Dispersion and Mechanical Properties of Polypropylene/Graphene Nanoplatelet Composites by Mixed Solvent-Assisted Melt Blending,” *Macromol. Res.*, 2020.

[99] C. Y. Su, A. Y. Lu, Y. Xu, F. R. Chen, A. N. Khlobystov, and L. J. Li, “High-quality thin graphene films from fast electrochemical exfoliation,” *ACS Nano*, 2011.

[100] S. N. Tripathi, G. S. S. Rao, A. B. Mathur, and R. Jasra, “Polyolefin/graphene nanocomposites: A review,” *RSC Adv.*, vol. 7, no. 38, pp. 23615–23632, 2017.

[101] Y. Huang, Y. Qin, Y. Zhou, H. Niu, Z. Z. Yu, and J. Y. Dong, “Polypropylene/graphene oxide nanocomposites prepared by in situ ziegler-natta polymerization,” *Chem. Mater.*, vol. 22, no. 13, pp. 4096–4102, 2010.

[102] M. A. Milani *et al.*, “Polypropylene/graphene nanosheet nanocomposites by in situ polymerization: Synthesis, characterization and fundamental properties,” *Compos. Sci. Technol.*, vol. 84, pp. 1–7, 2013.

[103] F. Liu *et al.*, “Synthesis of graphene materials by electrochemical exfoliation: Recent progress and future potential,” *Carbon Energy*. 2019.

[104] N. Kumar and V. C. Srivastava, “Simple Synthesis of Large Graphene Oxide Sheets via Electrochemical Method Coupled with Oxidation Process,” *ACS Omega*, 2018.

[105] K. Parvez *et al.*, “Exfoliation of graphite into graphene in aqueous solutions of inorganic salts,” *J. Am. Chem. Soc.*, 2014.

[106] A. M. Abdelkader, A. J. Cooper, R. A. W. Dryfe, and I. A. Kinloch, “How to get between the sheets: A review of recent works on the electrochemical exfoliation of graphene materials from bulk graphite,” *Nanoscale*. 2015.

[107] C. Gómez-Navarro *et al.*, “Electronic transport properties of individual chemically reduced graphene oxide sheets,” *Nano Lett.*, 2007.

[108] A. J. Cooper, N. R. Wilson, I. A. Kinloch, and R. A. W. Dryfe, “Single stage electrochemical exfoliation method for the production of few-layer graphene via intercalation of tetraalkylammonium cations,” *Carbon N. Y.*, 2014.

[109] C. Vilaverde, R. M. Santos, M. C. Paiva, and J. A. Covas, “Dispersion and re-agglomeration of graphite nanoplates in polypropylene melts under controlled flow conditions,” *Compos. Part A Appl. Sci. Manuf.*, 2015.

[110] A. A. Katbab, A. N. Hrymak, and K. Kasmadjian, “Preparation of interfacially compatibilized PP-EPDM thermoplastic vulcanizate/graphite nanocomposites: Effects of graphite microstructure upon morphology, electrical conductivity, and melt rheology,” *J. Appl. Polym. Sci.*, 2008.

[111] B. Li and W. H. Zhong, “Review on polymer/graphite nanoplatelet nanocomposites,” *Journal of Materials Science*. 2011.

[112] P. K. Ang, S. Wang, Q. Bao, J. T. L. Thong, and K. P. Loh, “High-throughput synthesis of graphene by intercalation-exfoliation of graphite oxide and study of

ionic screening in graphene transistor," *ACS Nano*, 2009.

[113] M. J. Allen, V. C. Tung, and R. B. Kaner, "Honeycomb carbon: A review of graphene," *Chem. Rev.*, 2010.

[114] I. Tantis, G. C. Psarras, and D. Tasis, "Functionalized graphene - poly(vinyl alcohol) nanocomposites: Physical and dielectric properties," *Express Polym. Lett.*, 2012.

[115] P. M. Ajayan and J. M. Tour, "Materials science: Nanotube composites," *Nature*. 2007.

[116] K. P. Pramoda, H. Hussain, H. M. Koh, H. R. Tan, and C. B. He, "Covalent bonded polymer-graphene nanocomposites," *J. Polym. Sci. Part A Polym. Chem.*, 2010.

[117] E. Cunha, M. C. Paiva, L. Hilliou, and J. A. Covas, "Tracking the progression of dispersion of graphite nanoplates in a polypropylene matrix by melt mixing," *Polym. Compos.*, vol. 38, no. 5, pp. 947–954, 2017.

[118] N. Xu, E. DIng, and F. Xue, "Influence of particle size of isotactic polypropylene (iPP) on barrier property against agglomeration of homogenized microcrystalline cellulose (HMCC) in iPP/HMCC composites," *J. Polym. Eng.*, 2018.

[119] V. A. González-González, G. Neira-Velázquez, and J. L. Angulo-Sánchez, "Polypropylene chain scissions and molecular weight changes in multiple extrusion *," *Polym. Degrad. Stab.*, 1998.

[120] J. L. White and H. B. Dee, "Flow visualization for injection molding of polyethylene and polystyrene melts," *Polym. Eng. Sci.*, 1974.

[121] J. Chu, M. R. Kamal, S. Derdouri, and A. Hrymak, "Characterization of the microinjection molding process," *Polym. Eng. Sci.*, vol. 50, no. 6, pp. 1214–1225, 2010.

[122] C. Yang, L. Li, H. Huang, J. M. Castro, and A. Y. Yi, “Replication characterization of microribs fabricated by combining ultraprecision machining and microinjection molding,” *Polym. Eng. Sci.*, 2010.

[123] I. Alig *et al.*, “Establishment, morphology and properties of carbon nanotube networks in polymer melts,” *Polymer*. 2012.

[124] T. Skipa, D. Lellinger, M. Saphiannikova, and I. Alig, “Shear-stimulated formation of multi-wall carbon nanotube networks in polymer melts,” *Phys. Status Solidi Basic Res.*, 2009.

[125] H. Pranov, H. K. Rasmussen, N. B. Larsen, and N. Gadegaard, “On the injection molding of nanostructured polymer surfaces,” *Polym. Eng. Sci.*, vol. 46, no. 2, pp. 160–171, 2006.

[126] A. Curtis and C. Wilkinson, “Nantotechniques and approaches in biotechnology,” *Trends in Biotechnology*, vol. 19, no. 3. pp. 97–101, 2001.

[127] N. Zhang, J. S. Chu, C. J. Byrne, D. J. Browne, and M. D. Gilchrist, “Replication of micro/nano-scale features by micro injection molding with a bulk metallic glass mold insert,” *J. Micromechanics Microengineering*, vol. 22, no. 6, 2012.

[128] M. Wang, W. Ding, Y. Xie, L. Zhang, and Y. Chen, “Effect of micro-mold cavity dimension on structure and property of polylactic acid/polycaprolactone blend under microinjection molding conditions,” *Polymers (Basel).*, 2021.

[129] M. A. Mohammad, M. Muhammad, S. K. Dew, and M. Stepanova, “Fundamentals of electron beam exposure and development,” in *Nanofabrication: Techniques and Principles*, vol. 9783709104, 2012, pp. 11–41.

[130] A. Allaoui, S. Bai, H. M. Cheng, and J. B. Bai, “Mechanical and electrical properties of a MWNT/epoxy composite,” *Compos. Sci. Technol.*, 2002.

[131] G. T. Pham *et al.*, “Mechanical and electrical properties of polycarbonate nanotube buckypaper composite sheets,” *Nanotechnology*, 2008.

[132] V. B. Mohan, K. Jayaraman, and D. Bhattacharyya, “Hybridization of graphene-reinforced two polymer nanocomposites,” *Int. J. Smart Nano Mater.*, 2016.

[133] A. Chanda, S. K. Sinha, and N. V. Datla, “Electrical conductivity of random and aligned nanocomposites: Theoretical models and experimental validation,” *Compos. Part A Appl. Sci. Manuf.*, 2021.

[134] S. Zhang *et al.*, “Carbon nanotube/carbon composite fiber with improved strength and electrical conductivity via interface engineering,” *Carbon N. Y.*, 2019.

[135] H. Lobo and J. V. Bonilla, *Handbook of Plastics Analysis*. 2003.

[136] H. Hu and G. Chen, “Electrochemically modified graphite nanosheets and their nanocomposite films with poly(vinyl alcohol),” *Polym. Compos.*, 2010.

[137] S. Kim, I. Do, and L. T. Drzal, “Thermal stability and dynamic mechanical behavior of exfoliated graphite nanoplatelets-LLDPE nanocomposites,” *Polym. Compos.*, 2010.

[138] J. Huang, T. Y. Wang, C. H. Wang, and Z. H. Rao, “Exfoliated graphite/paraffin nanocomposites as phase change materials for thermal energy storage application,” *Mater. Res. Innov.*, 2011.

[139] E. Assouline *et al.*, “Nucleation ability of multiwall carbon nanotubes in polypropylene composites,” *J. Polym. Sci. Part B Polym. Phys.*, 2003.

[140] D. G. Papageorgiou, K. Chrissafis, and D. N. Bikiaris, “β-Nucleated Polypropylene: Processing, Properties and Nanocomposites,” *Polym. Rev.*, 2015.

[141] D. Bikiaris, “Microstructure and properties of polypropylene/carbon nanotube nanocomposites,” *Materials*. 2010.

[142] M. El Achaby, F. E. Arrakhiz, S. Vaudreuil, A. El Kacem Qaiss, M. Bousmina, and O. Fassi-Fehri, “Mechanical, thermal, and rheological properties of graphene-based polypropylene nanocomposites prepared by melt mixing,” *Polym. Compos.*,

vol. 33, no. 5, pp. 733–744, 2012.

[143] M. V. Gudkov, N. G. Ryvkina, A. Y. Gorenberg, and V. P. Melnikov, “Electrically conductive nanocomposites with segregated structure based on poly(vinylidene fluoride-co-tetrafluoroethylene) and reduced graphene oxide,” *Dokl. Phys. Chem.*, 2016.

[144] J. Wang *et al.*, “Enhancing the electrical conductivity of PP/CNT nanocomposites through crystal-induced volume exclusion effect with a slow cooling rate,” *Compos. Part B Eng.*, 2020.

[145] G. Hu, C. Zhao, S. Zhang, M. Yang, and Z. Wang, “Low percolation thresholds of electrical conductivity and rheology in poly(ethylene terephthalate) through the networks of multi-walled carbon nanotubes,” *Polymer (Guildf).*, 2006.

[146] P. Pötschke, M. Abdel-Goad, I. Alig, S. Dudkin, and D. Lellinger, “Rheological and dielectrical characterization of melt mixed polycarbonate-multiwalled carbon nanotube composites,” *Polymer (Guildf).*, 2004.

[147] F. Du, R. C. Scogna, W. Zhou, S. Brand, J. E. Fischer, and K. I. Winey, “Nanotube networks in polymer nanocomposites: Rheology and electrical conductivity,” *Macromolecules*, 2004.

[148] O. Pekcan and G. Akn, “Conductivity Percolation of Carbon Nanotubes in Polyacrylamide Gels,” in *Carbon Nanotubes - Polymer Nanocomposites*, 2011.

[149] J. N. Martins, T. S. Bassani, G. M. O. Barra, and R. V. B. Oliveira, “Electrical and rheological percolation in poly(vinylidene fluoride)/multi-walled carbon nanotube nanocomposites,” *Polym. Int.*, 2011.

[150] E. Planes, J. Duchet, A. Maazouz, and J. F. Gerard, “Characterization of new formulations for the rotational molding based on ethylene-propylene copolymer/graphite nanocomposites,” *Polym. Eng. Sci.*, 2008.

[151] H. Kim and C. W. Macosko, “Processing-property relationships of

polycarbonate/graphene composites," *Polymer (Guildf).*, 2009.

[152] M. S. P. Shaffer and A. H. Windle, "Fabrication and characterization of carbon nanotube/poly(vinyl alcohol) composites," *Adv. Mater.*, 1999.

[153] S. Inoue, N. Ichikuni, T. Suzuki, T. Uematsu, and K. Kaneko, "Capillary condensation of N2 on multiwall carbon nanotubes," *J. Phys. Chem. B*, 1998.

[154] S. Zhou, A. N. Hrymak, and M. R. Kamal, "Electrical, thermal, and mechanical properties of polypropylene/multiwalled carbon nanotube micromoldings," *Polym. Compos.*, 2020.

[155] J. Park, E. Kyuyoung, O. Kwon, and S. Woo, "Chemical etching technique for the investigation of melt-crystallized isotactic polypropylene spherulite and lamellar morphology by scanning electron microscopy," *Microsc. Microanal.*, vol. 7, no. 3, pp. 276–286, 2001.

[156] S. A. Arvidson, S. A. Khan, and R. E. Gorga, "Mesomorphic-α-monoclinic phase transition in isotactic polypropylene: A study of processing effects on structure and mechanical properties," *Macromolecules*, 2010.

[157] S. T. Zhou, A. N. Hrymak, and M. R. Kamal, "Electrical, morphological and thermal properties of microinjection molded polypropylene/ multi-walled carbon nanotubes nanocomposites," *Int. Polym. Process.*, 2018.

[158] M. Wegrzyn, S. Juan, A. Benedito, and E. Giménez, "The influence of injection molding parameters on electrical properties of PC/ABS-MWCNT nanocomposites," *J. Appl. Polym. Sci.*, 2013.

[159] S. Zhou, A. N. Hrymak, and M. R. Kamal, "Microinjection molding of polypropylene/multi-walled carbon nanotube nanocomposites: The influence of process parameters," *Polym. Eng. Sci.*, 2018.

[160] M. K. H. Bhuiyan, M. M. Rahman, M. F. Mina, M. R. Islam, M. A. Gafur, and A. Begum, "Crystalline morphology and properties of multi-walled carbon nanotube

filled isotactic polypropylene nanocomposites: Influence of filler size and loading," *Compos. Part A Appl. Sci. Manuf.*, 2013.

[161] P. G. Ren *et al.*, "Synergetic toughening effect of carbon nanotubes and β-nucleating agents on the polypropylene random copolymer/styrene-ethylene-butylene- styrene block copolymer blends," *Polymers (Basel).*, 2018.

[162] J. Chen, X. Li, and C. Wu, "Crystallization behavior of polypropylene filled with modified carbon black," *Polym. J.*, 2007.

[163] Z. Zhou, S. Wang, Y. Zhang, and Y. Zhang, "Effect of different carbon fillers on the properties of PP composites: Comparison of carbon black with multiwalled carbon nanotubes," *J. Appl. Polym. Sci.*, 2006.

[164] S. Zhou, A. N. Hrymak, and M. R. Kamal, "Effect of hybrid carbon fillers on the electrical and morphological properties of polystyrene nanocomposites in microinjection molding," *Nanomaterials*, 2018.

[165] A. Dorigato, M. Brugnara, and A. Pegoretti, "Synergistic effects of carbon black and carbon nanotubes on the electrical resistivity of poly(butylene-terephthalate) nanocomposites," *Adv. Polym. Technol.*, 2018.

[166] P. Pötschke, T. D. Fornes, and D. R. Paul, "Rheological behavior of multiwalled carbon nanotube/polycarbonate composites," *Polymer (Guildf).*, 2002.

[167] X. Tuo, G. Ma, Q. Tan, Y. Gong, and J. Guo, "A study on dispersions of CB and CNT in PP/EPDM composites and their mechanical reinforcement," *Polym. Polym. Compos.*, 2020.

[168] J. Sumfleth, S. T. Buschhorn, and K. Schulte, "Comparison of rheological and electrical percolation phenomena in carbon black and carbon nanotube filled epoxy polymers," *J. Mater. Sci.*, 2011.

[169] M. M. A. Nassar *et al.*, "Polymer powder and pellets comparative performances as bio-based composites," *Iran. Polym. J. (English Ed.*, 2021.

[170] S. Zhou, A. N. Hrymak, M. R. Kamal, and R. Jiang, “Properties of microinjection-molded polypropylene/graphite composites,” *Polym. Eng. Sci.*, 2019.

[171] B. H. Cipriano *et al.*, “Conductivity enhancement of carbon nanotube and nanofiber-based polymer nanocomposites by melt annealing,” *Polymer (Guildf).*, 2008.

[172] E. Tarani, G. Z. Papageorgiou, D. N. Bikiaris, and K. Chrissafis, “Kinetics of crystallization and thermal degradation of an isotactic polypropylene matrix reinforced with graphene/glass-fiber filler,” *Molecules*, 2019.

[173] W. Zheng, X. Lu, C. L. Toh, T. H. Zheng, and C. He, “Effects of clay on polymorphism of polypropylene in polypropylene/clay nanocomposites,” *J. Polym. Sci. Part B Polym. Phys.*, 2004.

Appendices

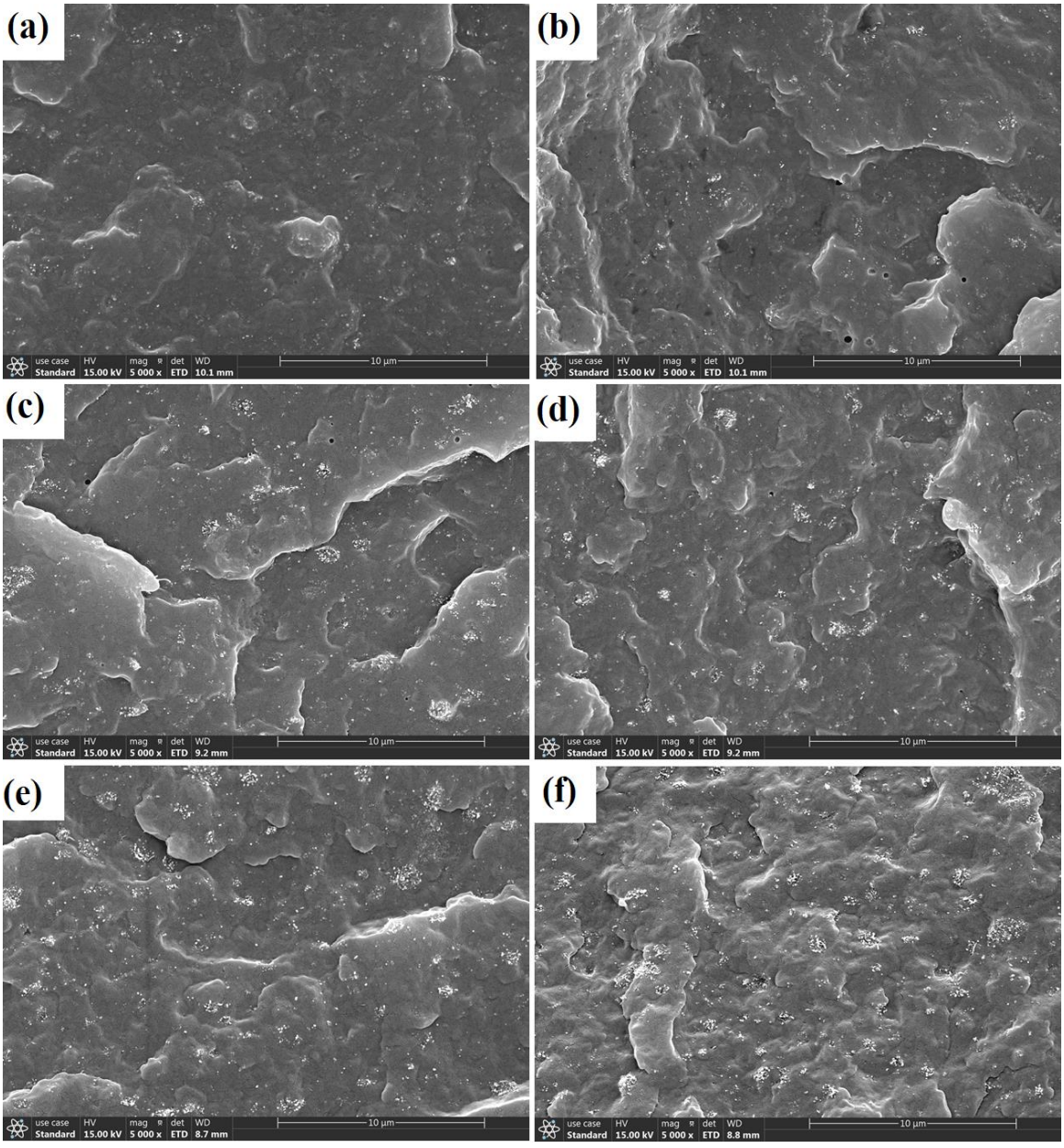

Appendix A: SEM images of (a, b) PP/(CNT30:CB70)3T microparts; (c, d) PP/(CNT50:CB50)3T microparts; (e, f) PP/(CNT70:CB30)3T microparts. Herein: (a) skin layer (b) core layer

Curriculum Vitae

Name: Renze Jiang

Post-secondary Education and Degrees:

University of Western Ontario
London, Ontario, Canada
2019-2021 M.E.Sc in Chemical Engineering

The University of Western Ontario
London, Ontario, Canada
2014-2019 B.E.Sc in Chemical Engineering

Honours and Awards:

Ontario Graduate Scholarship
2019-2021

Graduate with Distinction
2019

John M. Thompson Award in Engineering Leadership and Innovation
2019

Related Work Experience

Graduate Research Assistant
The University of Western Ontario
2019-2021

Graduate Teaching Assistant
The University of Western Ontario
2020

Process Engineering Intern
GreenMantra Technologies
2017-2018

Inside Sales and Engineering Intern
HTS Engineering
2017

Publications:

Zhou, S., Hrymak, A. N., Kamal, M. R. & Jiang, R. Properties of microinjection-molded polypropylene/graphite composites. Polym. Eng. Sci. (2019). doi:10.1002/pen.25154